with these antiviral drugs. On the other hand, most patients with chronic HBV infection achieve sufficient viral suppression and disease quiescence through immunological suppression of the virus. As we showed in this study, the immunological suppression of HBV is much stronger than that achieved with IFN therapy, but it is often transient. It is thus necessary to clarify the mechanism of transient immune response and to develop treatment that produces persistent suppression of HBV. Quantitative measurement of hypermutated genomes should be useful in monitoring the immune response in this context.

Acknowledgments

We thank Rie Akiyama, Miyuki Matsushita, and Yoshiko Seo for excellent technical assistance and Yoshiko Nakata for secretarial assistance.

References

1. Wright TL, Lau JYN. Clinical aspects of hepatitis B virus infection. Lancet **1993**; 342:1340–4.
2. Ganem D, Prince AM. Hepatitis B virus infection: natural history and clinical consequences. N Engl J Med **2004**; 350:1118–29.
3. Bruix J, Llovet JM. Hepatitis B virus and hepatocellular carcinoma. J Hepatol **2003**; 39(Suppl 1):S59–63.
4. Sheehy AM, Gaddis NC, Choi JD, Malim MH. Isolation of a human gene that inhibits HIV-1 infection and is suppressed by the viral Vif protein. Nature **2002**; 418:646–50.
5. Mangeat B, Turelli P, Caron G, Friedli M, Perrin L, Trono D. Broad antiretroviral defence by human APOBEC3G through lethal editing of nascent reverse transcripts. Nature **2003**; 424:99–103.
6. Zhang HYB, Pomerantz RJ, Zhang C, Arunachalam SC, Gao L. The cytidine deaminase CEM15 induces hypermutation in newly synthesized HIV-1 DNA. Nature **2003**; 424:94–8.
7. Lecossier D, Bouchonnet F, Clavel F, Hance AJ. Hypermutation of HIV-1 DNA in the absence of the Vif protein. Science **2003**; 300:1112.
8. Harris RS, Bishop KN, Sheehy AM, et al. DNA determination mediates innate immunity to retroviral infection. Cell **2003**; 113:803–9.
9. Liu B, Yu X, Luo K, Yu Y, Yu XF. Influence of primate lentiviral vif and proteasome inhibitors on human immunodeficiency virus type 1 virion packaging of APOBEC3G. J Virol **2004**; 78:2072–81.
10. Mehle A, Strack B, Ancuta P, Zhang C, McPike M, Gabuzda D. Vif overcomes the innate antiviral activity of APOBEC3G by promoting its degradation in the ubiquitin-proteasome pathway. J Biol Chem **2004**; 279:7792–8.
11. Marin M, Rose KM, Kozak SL, Kabat D. HIV-1 Vif protein binds the editing enzyme APOBEC3G and induces its degradation. Nat Med **2003**; 9:1398–403.
12. Stopak K, de Noronha C, Yonemoto W, Greene WC. HIV-1 Vif blocks the antiviral activity of APOBEC3G by impairing both its translation and intracellular stability. Mol Cell **2003**; 12:591–601.
13. Zack JA, Arrigo SJ, Weitsman SR, Go AS, Haislip A, Chen IS. HIV-1 entry into quiescent primary lymphocytes: molecular analysis reveals a labile, latent viral structure. Cell **1990**; 61:213–22.
14. Korin YD, Zack JA. Progression to the G1b phase of the cell cycle is required for completion of human immunodeficiency virus type 1 reverse transcription in T cells. J Virol **1998**; 72:3161–8.
15. Pierson TC, Zhou Y, Kieffer TL, Ruff CT, Buck C, Siliciano RF. Molecular characterization of preintegration latency in human immunodeficiency virus type 1 infection. J Virol **2002**; 76:8518–31.
16. Stevenson M, Stanwick TL, Dempsey MP, Lamonica CA. HIV-1 replication is controlled at the level of T cell activation and proviral integration. EMBO J **1990**; 9:1551–60.
17. Chiu YL, Soros VB, Kreisberg JF, Stopak K, Yonemoto W, Greene WC. Cellular APOBEC3G restricts HIV-1 infection in resting CD4$^+$ T cells. Nature **2005**; 435:108–14.
18. Tanaka Y, Marusawa H, Seno H, et al. Antiviral protein APOBEC3G is induced by interferon-alpha stimulation in human hepatocytes. Biochem Biophys Res Commun **2006**; 341:314–9.
19. Peng G, Lei KJ, Jin W, Greenwell-Wild T, Wahl SM. Induction of APOBEC3 family proteins, a defensive maneuver underlying interferon-induced anti-HIV-1 activity. J Exp Med **2006**; 203:41–6.
20. Bonvin M, Achermann F, Greeve I, et al. Interferon-inducible expression of APOBEC3 editing enzymes in human hepatocytes and inhibition of hepatitis B virus replication. Hepatology **2006**; 43:1364–74.
21. Chen K, Huang J, Zhang C, et al. Alpha interferon potently enhances the anti-human immunodeficiency virus type 1 activity of APOBEC3G in resting primary CD4 T cells. J Virol **2006**; 80:7645–57.
22. Newman EN, Holmes RK, Craig HM, et al. Antiviral function of APOBEC3G can be dissociated from cytidine deaminase activity. Curr Biol **2005**; 15:166–70.
23. Navarro F, Bollman B, Chen H, et al. Complementary function of the two catalytic domains of APOBEC3G. Virology **2005**; 333:374–86.
24. Nguyen DH, Gummuluru S, Hu J. Deamination-independent inhibition of hepatitis B virus reverse transcription by APOBEC3G. J Virol **2007**; 81:4465–72.
25. Gunther S, Sommer G, Plikat U, Iwanska A, WainHobson S, Will H, et al. Naturally occurring hepatitis B virus genomes bearing the hallmarks of retroviral G→A hypermutation. Virology **1997**; 235:104–8.
26. Suspene R, Guetard D, Henry M, Sommer P, Wain-Hobson S, Vartanian JP. Extensive editing of both hepatitis B virus DNA strands by APOBEC3 cytidine deaminases in vitro and in vivo. Proc Natl Acad Sci U S A **2005**; 102:8321–6.
27. Noguchi C, Ishino H, Tsuge M, et al. G to A hypermutation of hepatitis B virus. Hepatology **2005**; 41:626–33.
28. Noguchi C, Hiraga N, Mori N, et al. Dual effect of APOBEC3G on hepatitis B virus. J Gen Virol **2007**; 88:432–40.
29. Desmet VJ, Gerber M, Hoofnagle JH, Manns M, Scheuer PJ. Classification of chronic hepatitis: diagnosis, grading and staging. Hepatology **1994**; 19:1513–20.
30. Norder H, Courouce AM, Magnius LO. Complete genomes, phylogenetic relatedness, and structural proteins of 6 strains of the hepatitis-B virus, 4 of which represent 2 new genotypes. Virology **1994**; 198:489–503.
31. Tsuge M, Hiraga N, Takaishi H, et al. Infection of human hepatocyte chimeric mouse with genetically engineered hepatitis B virus. Hepatology **2005**; 42:1046–54.
32. Tateno C, Yoshizane Y, Saito N, et al. Near completely humanized liver in mice shows human-type metabolic responses to drugs. Am J Pathol **2004**; 165:901–12.

Toxicology and Applied Pharmacology 237 (2009) 119–126

Contents lists available at ScienceDirect

Toxicology and Applied Pharmacology

journal homepage: www.elsevier.com/locate/ytaap

CYP1A1 and CYP1A2 expression: Comparing 'humanized' mouse lines and wild-type mice; comparing human and mouse hepatoma-derived cell lines

Shigeyuki Uno [a], Kaori Endo [a], Yuji Ishida [b], Chise Tateno [b], Makoto Makishima [a], Katsutoshi Yoshizato [b], Daniel W. Nebert [c,*]

[a] Department of Biochemistry, Nihon University School of Medicine, 30-1 Oyaguchikami-cho, Itabashi-ku, Tokyo 173-8610, Japan
[b] PhenixBio Co., Ltd., 3-4-1 Kagamiyama, Higashihiroshima, Hiroshima 739-0046, Japan
[c] Department of Environmental Health and Center for Environmental Genetics (CEG) University of Cincinnati Medical Center, P.O. Box 670056, Cincinnati OH 45267-0056, USA

ARTICLE INFO

Article history:
Received 17 November 2008
Revised 10 February 2009
Accepted 2 March 2009
Available online 10 March 2009

Keywords:
Cytochrome P450 1 (*CYP1*) genes
Bacterial artificial chromosome (BAC)
hCYP1A1_1A2_Cyp1a1/1a2(−/−) BAC-transgenic mouse line
uPA/SCID chimeric mouse line carrying human hepatocytes
Human risk assessment
Western immunoblot
Benzo[*a*]pyrene hydroxylase, ethoxyresorufin *O*-deethylase, acetanilide 4-hydroxylase and methoxyresorufin *O*-demethylase as CYP1A1 and CYP1A2 substrates
2,3,7,8-Tetrachlorodibenzo-*p*-dioxin (TCDD, dioxin) as P450 inducer
Mouse Hepa-1c1c7 cell culture
Human HepG2 cell culture

ABSTRACT

Human and rodent cytochrome P450 (**CYP**) enzymes sometimes exhibit striking species-specific differences in substrate preference and rate of metabolism. Human risk assessment of CYP substrates might therefore best be evaluated in the intact mouse by replacing mouse *Cyp* genes with human *CYP* orthologs; however, how "human-like" can human gene expression be expected in mouse tissues? Previously a bacterial-artificial-chromosome-transgenic mouse, carrying the human *CYP1A1_CYP1A2* locus and lacking the mouse *Cyp1a1* and *Cyp1a2* orthologs, was shown to express robustly human dioxin-inducible CYP1A1 and basal versus inducible CYP1A2 (mRNAs, proteins, enzyme activities) in each of nine mouse tissues examined. Chimeric mice carrying humanized liver have also been generated, by transplanting human hepatocytes into a urokinase-type plasminogen activator(+/+)_severe-combined-immunodeficiency (*uPA/SCID*) line with most of its mouse hepatocytes ablated. Herein we compare basal and dioxin-induced CYP1A mRNA copy numbers, protein levels, and four enzymes (benzo[*a*]pyrene hydroxylase, ethoxyresorufin *O*-deethylase, acetanilide 4-hydroxylase, methoxyresorufin *O*-demethylase) in liver of these two humanized mouse lines versus wild-type mice; we also compare these same parameters in mouse Hepa-1c1c7 and human HepG2 hepatoma-derived established cell lines. Most strikingly, mouse liver CYP1A1-specific enzyme activities are between 38- and 170-fold higher than human CYP1A1-specific enzyme activities (per unit of mRNA), whereas mouse versus human CYP1A2 enzyme activities (per unit of mRNA) are within 2.5-fold of one another. Moreover, both the mouse and human hepatoma cell lines exhibit striking differences in CYP1A mRNA levels and enzyme activities. These findings are relevant to risk assessment involving human CYP1A1 and CYP1A2 substrates, when administered to mice as environmental toxicants or drugs.

Introduction

The human and mouse genomes comprise 57 and 102 protein-coding cytochrome P450 (**CYP**) genes, respectively, each divided into 18 families (Nelson et al., 2004; Nebert et al., 2004; Nebert and Dalton, 2006). The mammalian *CYP1* gene family encodes three enzymes in both human and mouse—CYP1A1, CYP1A2 and CYP1B1. While the *CYP1A* and *CYP1B* subfamily ancestors diverged from one another ~480 million years ago, *CYP1A2* arose as a duplication event from the *CYP1A1* gene about 420 million years ago. Thus, land animals (including birds) carry both *CYP1A1* and *CYP1A2*; on the other hand, fish genomes do not contain the *CYP1A2* gene (Nelson et al., 1996).

It was originally noted that alteration of a single amino-acid in a CYP protein could change dramatically its catalytic activity from coumarin to testosterone hydroxylation (Lindberg and Negishi, 1989). Similarly, numerous other examples have shown that human and rodent CYP1A2 orthologs, having important amino-acid differences, can display striking species-specific variability in the rates by which certain substrates are metabolized (Turesky, 2005). For example, human and mouse CYP1A2 differ by 3- to 7-fold in catalyzing ethoxyresorufin *O*-deethylation (Aoyama et al., 1989) and uroporphyrinogen oxidation (Nichols et al., 2003).

It therefore can be difficult to extrapolate toxicity or cancer data from rodent studies to human risk assessment. For this reason, we and others have generated "humanized" *hCYP1A1_1A2* transgenic lines in which either mouse *Cyp1a1* or *Cyp1a2* (Jiang et al., 2005; Cheung et al., 2005; Derkenne et al., 2005) or both mouse *Cyp1a1* and *Cyp1a2* (Dragin et al., 2007; Shi et al., 2008) orthologs are

* Corresponding author. Fax: +1 513 558 0974.
E-mail address: dan.nebert@uc.edu (D.W. Nebert).

0041-008X/$ – see front matter © 2009 Published by Elsevier Inc.
doi:10.1016/j.taap.2009.03.001

ablated. In addition, a global approach for making a humanized mouse has been developed by transplanting human hepatocytes into the urokinase-type plasminogen activator(+/+)_severe-combined-immunodeficiency (*uPA/SCID*) mouse, which otherwise is immunodeficient and undergoes liver failure; these chimeric mice no longer develop liver failure, but rather the mouse liver comprises >70% human hepatocytes that propagate successfully and retain normal pharmacological functions such as drug metabolism (Tateno et al., 2004; Katoh et al., 2008). Eight human P450s (CYP1A2, 2A6, 2C8, 2C9, 2C19, 2D6, 3A4, 3A5), 35 other Phase I enzymes, and four classes of Phase II conjugating enzymes (UDP glucuronosyltransferases, glutathione *S*-transferases, *N*-acetyltransferases, and sulfotransferases) have been shown to be functional in chimeric mice (Katoh et al., 2008). Because each chimeric mouse will reflect the liver profile and genetic makeup of the human donor's hepatocytes, interindividual and ethnic differences in drug metabolism will undoubtedly exist. Nevertheless, variations of xenobiotic-metabolizing enzymes as well as other enzymes, receptors, transporters, transcription factors, and any other drug target located in human liver—might effectively be studied in such chimeric mouse lines.

Mammalian CYP1A1 basal mRNA is known to be negligible, resulting in no detectable CYP1A1 protein in any tissue, whereas basal levels of CYP1A2 mRNA and protein are relatively high in liver but generally low (protein undetectable on Western immunoblot) in nonhepatic tissues; induction by a CYP1 inducer such as chemicals in cigarette smoke or 2,3,7,8-tetrachlorodibenzo-*p*-dioxin (**TCDD**; **dioxin**) increases CYP1A1 and CYP1A2 mRNA and protein levels (Eaton et al., 1995; Nebert et al., 2004). Recently, two humanized *CYP1A1_1A2* lines were compared with C57BL/6J (**B6**) inbred mice with regard to expression of CYP1A1 and CYP1A2 mRNA levels following TCDD pretreatment. Maximally-induced mRNA concentrations of mouse CYP1A1 were ~10 times higher in liver and lung and ~100-fold greater in kidney than those of human CYP1A1 (Shi et al., 2008). On the other hand, maximally-induced mRNA levels of mouse CYP1A2 in liver were <2-fold higher than those of human CYP1A2. Maximally-induced mRNA levels of human CYP1A2 in liver were ~12 times higher than those of human CYP1A1, whereas maximally-induced mRNA levels of mouse CYP1A2 in liver were ~3-fold greater than those of mouse CYP1A1 (Shi et al., 2008).

These data caused us to query how "physiologically" relevant these human mRNA levels might be, in the intact mouse. Do these humanized mouse lines actually reflect "average" *CYP1A1* and *CYP1A2* gene expression that might be expected among individuals in a human population, or is this expression abnormally low or high? One should be able to shed some light on this, by comparing precise copy numbers of basal and TCDD-induced CYP1A1 and CYP1A2 mRNA (combined with quantification of protein levels and enzyme assays) in the humanized mouse lines versus wild-type mice.

Those who oppose the use of laboratory animals, and recommend instead that everyone utilize cells in culture, often declare that studies with cultured cell lines can provide information that would accurately reflect what is found in the intact animal. We therefore have compared the above-mentioned CYP1A1 and CYP1A2 parameters in liver from the humanized mouse lines and wild-type mice with those in human versus mouse hepatoma-derived established cell culture lines. The present study addresses these questions. Answering these questions should be beneficial, before launching into human risk assessment studies using such humanized mouse lines.

Material and methods

Mice. C57BL/6J (B6) mice were purchased from The Jackson Laboratory (Bar Harbor, ME). Development of the humanized *hCYP1A1_1A2_Cyp1a1/1a2(−/−)-Ahr*^{b1} transgenic line has been detailed (Dragin et al., 2007). Chimeric mice bearing human hepatocytes were generated using *uPA(+/+)/SCID* mice as the host (Giannini et al., 2003) and characterized (Tateno et al., 2004; Katoh et al., 2008); their human hepatocyte-replacement rates were between 73% and 83%. All experiments involving mice adhered to the Guidelines for Animal Experiments and Use Committee of the Nihon University School of Medicine.

Treatment of mice. Mice were treated with intraperitoneal TCDD (25 μg/kg for 24 h), versus corn oil vehicle alone for untreated. At least three groups ($N = 3$ each time) were studied to ensure reproducibility.

Cell cultures and treatment. The human HepG2 established cell line was derived from a hepatoblastoma (Dearfield et al., 1983). The mouse Hepa-1c1c7 line was derived from a C57L/J hepatoma (Bernhard et al., 1973). Cultured cells were treated with 10 nM TCDD for 24 h before total RNA isolation.

Reverse transcription. Total RNAs from samples were prepared by the acid guanidine thiocyanate-phenol/chloroform method (Tavangar et al., 1990). The cDNAs were synthesized using the ImProm-II Reverse Transcription system (Promega, Madison, WI) (Inaba et al., 2007).

Quantitative real-time PCR (qRT-PCR). We used the primers listed in Table 1. The qRT-PCR was performed in an ABI PRISM 7000 Sequence Detection System™ (Applied Biosystems), using Power SYBR Green PCR Master Mix (Applied Biosystems). Individual CYP1 mRNA abundance was determined, using the standard-curve method (from 10^1 to 10^8 copies/μL), as previously described by K. Livak (PE-ABI; Sequence Detector User; Bulletin #2) (Winer et al., 1999). Each sample was normalized to mouse glyceraldehyde-3-phosphate dehydrogenase (**GAPDH**) mRNA.

CYP1A mRNA copy numbers. Transcripts from the human *CYP1A1* and *CYP1A2* and the mouse *Cyp1a1* and *Cyp1a2* genes were quantified by fitting qRT-PCR data to a curve generated from cloned RNAs (cRNAs) for each CYP1. Briefly described, templates for cRNA synthesis were produced by PCR on cDNA constructs from each CYP1A cDNA that had been cloned into pcDNA3.1(+) (Invitrogen), using T7 RiboMAX™ Express Large-Scale RNA Production System (Promega) (Uno et al., 2006). The cRNAs were used to generate a standard curve in the PCR reactions from which mRNA copy numbers from qRT-RNA measurements could be extrapolated.

Western immunoblot analysis. Mice were euthanized by carbon dioxide asphyxiation followed by cervical dislocation. The liver was excised, and microsomes were prepared as previously described (Dalton et al., 2000). Protein concentrations were determined by the bicinchoninic acid method (Pierce Chemical Co.; Rockford, IL), according to details provided by the manufacturer. Microsomal proteins were separated on sodium dodecylsulfate (0.1%)–polyacrylamide (12%) minigels. Separated proteins were transferred to nitrocellulose membranes. Western immunoblot analysis was performed using goat polyclonal anti-rat CYP1A1/1A2 antibody; this antibody (Daiichi Pure Chemicals, Tokyo, Japan) recognizes both the human and mouse CYP1A1 and CYP1A2 proteins. We used alkaline phosphatase-conjugated secondary antibodies (Kirkegaard Perry Lab., Gaithersburg, MD) and the Alkaline

Table 1
Primer pairs used in qRT-PCR.

Gene	Forward primer	Reverse primer
hCYP1A1	5′-AAGGGGCGTTGTGTCTTTGT-3′	5′-ATACACTTCCGCTTGCCCAT-3′
hCYP1A2	5′-ACAAGGGACACAACGCTGAA-3′	5′-AGGGCTTGTTAATGGCAGTG-3′
mCyp1a1	5′-CCTCATGTACCTGGTAACCA-3′	5′-AAGGATGAATGCCGGAAGGT-3′
mCyp1a2	5′-AAGACAATGGCGGTCTCATC-3′	5′-GACGGTCAGAAAGCCGTGGT-3′
mGapdh	5′-TGCACCACCAACTGCTTAG-3′	5′-GATGCAGGGATGATGTTC-3′

h, human; m, mouse.

Phosphatase Conjugate Substrate Kit™ (Bio-Rad Lab., Hercules, CA), with exposure times ranging from 5 to 10 min.

Enzyme assays. Determination of microsomal BaP hydroxylase (Nebert and Gelboin, 1968) and ethoxyresorufin *O*-deethylase (**EROD**) (Burke et al., 1977) activities principally represent CYP1A1 activity. Acetanilide 4-hydroxylase (Shertzer et al., 2001) and methoxyresorufin *O*-demethylase (**MROD**) (Berthou et al., 1992; Hamm et al., 1998; Shertzer et al., 2001) activities principally (but not exclusively) represent CYP1A2 activity. These enzymes were assayed by the methods cited. Although the MROD spectrophotofluororometric assay is sensitive and reliable, it has been demonstrated (Hamm et al., 1998) that the MROD assay is not the most suitable for estimating CYP1A2 activity. In *Cyp1a2(−/−)* knockout mice, it was shown that hepatic MROD activity was increased 70-fold by TCDD treatment, indicating that other TCDD-inducible enzymes contribute to inducible MROD activity. In contrast, acetanilide 4-hydroxylase activity in *Cyp1a2(−/−)* knockout mice was induced only 2-fold by dioxin (Shertzer et al., 2001), suggesting that it is by far the preferred enzyme activity for estimating CYP1A2 catalytic expression.

Biohazard precaution. TCDD is highly toxic and regarded as a likely human carcinogen. All personnel were instructed in safe handling procedures. Lab coats, gloves and masks were worn at all times, and contaminated materials were collected separately for disposal by the Hazardous Waste Unit or by independent contractors. TCDD-treated mice were housed separately, and their carcasses regarded as contaminated biological materials. TCDD-treated cells in culture, and culture medium from these cells, were also regarded as contaminated biological materials.

Statistical analysis. Statistical significance between groups was determined by analysis-of-variance among groups and Student's *t*-test between groups. All assays were performed in duplicate or triplicate, and repeated at least twice. Statistical analyses were also carried out with the use of SAS® statistical software (SAS Institute Inc.; Cary, NC) and Sigma Plot (Systat Software, Inc., Point Richmond, CA).

Results and discussion

Factors affecting CYP expression

In a previous study of the entire gastrointestinal tract (Uno et al., 2008), large differences in basal but especially inducible CYP1A1 and CYP1A2 mRNA and protein levels were seen. This variability appears to depend on the route-of-administration and the target organ being studied: oral versus intraperitoneal administration of TCDD or BaP can drastically alter CYP1 mRNA levels in various cell types of the intestine, from tongue to colon (Uno et al., 2008). In two studies comparing humanized mice with wild-type controls (Dragin et al., 2007; Shi et al., 2008), large differences were also observed in human CYP1A1 or CYP1A2 mRNA, compared with mouse CYP1A1 or CYP1A2 mRNA. In the chimeric *uPA/SCID* humanized mouse, although CYP1A1 was not studied, large variability in CYP1A2 expression has also been seen (Katoh et al., 2008).

Reasons for differences in human transgene expression in humanized mouse tissues include: [a] genotype of the volunteer from whom the BAC library was derived (Jiang et al., 2005) or from whose hepatocytes were infused into a *uPA(+/+)/SCID* mouse (Katoh et al., 2008; [b] chromosomal location of the randomly inserted BAC transgene affecting transgene expression, *i.e.* the "neighborhood effect" (Bedell et al., 1996; Milot et al., 1996; Olson et al., 1996; Muller et al., 2001); [c] genetic background (modifier genes) of a particular inbred strain that can influence transgene expression (Bonyadi et al., 1997; Cranston and Fishel, 1999; Bennett et al., 2000); and [d] a BAC containing the human gene(s) (Jiang et al., 2005; Cheung et al., 2005) which does not include *trans*-regulatory, or all of the *cis*-regulatory, sites needed for "normal" expression of the transgene(s) in each mouse tissue or cell type studied.

Comparison of human versus mouse CYP1A1 mRNA levels in liver

Fig. 1A compares human and mouse CYP1A1 mRNA copy numbers in the *hCYP1A1_1A2_Cyp1a1/1a2(−/−)* line, B6 wild-type mice containing no human transgenes, chimeric *uPA/SCID* mice (**chimera**), and *uPA(+/+)/SCID* control mice containing no human hepatocytes (*uPA/SCID* mice). Human basal CYP1A1 mRNA levels in the liver of *hCYP1A1_1A2* and chimeric mice were quite low, having $\sim 1.3\times 10^7$ and $\sim 1.2\times 10^7$ transcript copy numbers (per μg total RNA), respectively; both were strikingly increased by TCDD to $\sim 7.3\times 10^9$ and $\sim 2.0\times 10^9$ copy numbers, respectively.

Mouse basal CYP1A1 mRNA levels in B6, chimeric, and *uPA/SCID* mice (Fig. 1A) were also quite low ($\sim 1.8\times 10^6$, $\sim 1.7\times 10^6$, and 1.0×10^6 copy numbers, respectively), but all were dramatically induced by TCDD to $\sim 2.5\times 10^8$, $\sim 8.0\times 10^7$, and $\sim 1.5\times 10^8$ copy numbers, respectively. As expected, no human CYP1A1 mRNA was detected in B6 or *uPA/SCID* mice, and no mouse CYP1A1 mRNA was detected in the *hCYP1A1_1A2_Cyp1a1/1a2(−/−)* line.

Comparison of human versus mouse CYP1A2 mRNA levels in liver

Human basal CYP1A2 mRNA levels in *hCYP1A1_1A2_Cyp1a1/1a2(−/−)* and chimeric mice (Fig. 1B) were low ($\sim 2.6\times 10^8$ and $\sim 0.89\times 10^8$ transcript copy numbers, respectively). Both were significantly elevated by TCDD to $\sim 9.7\times 10^8$ and $\sim 7.7\times 10^8$ copy numbers, respectively.

Mouse basal CYP1A2 mRNA concentrations in B6, chimeric, and *uPA/SCID* mice were also low ($\sim 2.2\times 10^8$, $\sim 0.16\times 10^8$ and $\sim 1.2\times 10^8$ copy numbers, respectively); all three were significantly induced by TCDD to $\sim 4.2\times 10^9$, $\sim 0.73\times 10^9$, and 2.8×10^9 copy numbers, respectively (Fig. 1B). As expected, no human CYP1A2 mRNA was detected in B6 and *uPA/SCID* mice, and no mouse CYP1A2 mRNA was detected in the *hCYP1A1_1A2_Cyp1a1/1a2(−/−)* line.

Comparison of human versus mouse CYP1A1 and CYP1A2 mRNA levels

It should be noted that the basal expression levels of human and mouse CYP1A2 mRNA ($1–3\times 10^8$ copy numbers) were much higher (Fig. 1) than those of CYP1A1 mRNA ($\sim 10^7$ copy numbers). This conclusion supports the results of studies long ago (Nebert, 1989; Eaton et al., 1995). The induction of human and mouse CYP1A1 and CYP1A2 mRNAs by TCDD is also well known (Nebert, 1989; Eaton et al., 1995; Nebert et al., 2004).

A previous report (Shi et al., 2008) compared the expression of CYP1A1 and CYP1A2 mRNA in liver between two humanized *CYP1A1_1A2_Cyp1a1/1a2(−/−)* lines and the B6 inbred mouse: maximally-induced mRNA levels of mouse CYP1A1 were described as ~10 times higher than those of human CYP1A1; in contrast, maximally-induced mRNA levels of mouse CYP1A2 were <2-fold higher than those of human CYP1A2 in liver. However, the present study (in which we find a mouse/human induced CYP1A1 ratio of ~0.03 and a mouse/human induced CYP1A2 ratio of ~4) appears not to be consistent with this previous report.

The previous report also found that maximally-induced mRNA levels of human CYP1A2 in liver were ~12 times higher than those of human CYP1A1, whereas maximally-induced mRNA levels of mouse CYP1A2 were ~3-fold greater than those of mouse CYP1A1 (Shi et al., 2008). In the present study, these ratios are 0.13 and 16.8, respectively. These large differences in the calculated ratios clearly reflect the

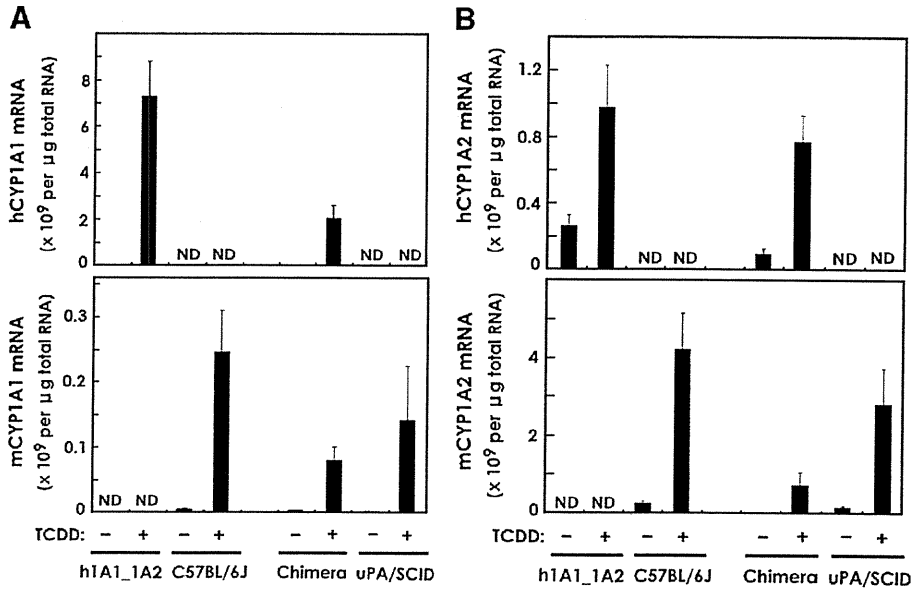

Fig. 1. Human (*upper panels*) versus mouse (*lower panels*) CYP1A1 (A) and CYP1A2 (B) mRNA copy numbers in liver from the *hCYP1A1_1A2_Cyp1a1/1a2(−/−)_Ahr*^{b1} mouse line, B6 inbred mouse, chimeric mouse, and *uPA/SCID* mouse—with, versus without, TCDD pretreatment. When administered, TCDD (25 µg/kg body weight 24 h before killing) was given intraperitoneally. "**ND**" (nondetectable by qRT-PCR) denotes nothing above background, whereas absence of "ND" (detectable, but extremely low by qRT-PCR) denotes something measurable above background. On *Y*-axis: **h**CYP1A1 or **h**CYP1A2 = human mRNA; **m**CYP1A1 or **m**CYP1A2 = mouse mRNA. For this figure and Fig. 4, the method for determining the copy number of mRNA molecules per µg total RNA is given in "Materials & methods". Note the different labels on the *Y*-axes of these figures. *Bars* and *brackets* denote means ± S.E.M., respectively ($N=3$ independent experiments).

disparity between the "relative values" given in the previous report and the "absolute values" (*i.e.* copy numbers per µg total RNA) in the present study.

Human induced and basal CYP1A2 mRNA copy numbers in chimeric mice were 73–80% lower than those in *uPA/SCID* mice (Fig. 1B). This decrease can easily be explained when the human hepatocyte-replacement rate (73%–83%) is taken into account. This finding supports the notion that human hepatocytes in chimeric mice liver are affected by TCDD independently from mouse hepatocytes, suggesting that human hepatocytes in chimeric mice liver can mimic those in human liver.

The induction rate (Fig. 1) of human CYP1A1 mRNA in the *hCYP1A1_1A2_Cyp1a1/1a2(−/−)* line is quite remarkable (>500-fold), whereas that in chimeric mouse was not nearly as high (~170-fold). In contrast, the induction rate of human CYP1A2 mRNA in *hCYP1A1_1A2_Cyp1a1/1a2(−/−)* mice was ~3.7-fold, whereas that in the chimera was higher (~8.7-fold). These differences in fold-induction could be due to differences in the transcription regulatory regions associated with each of the two genes—if we assume that human and mouse genomic regulatory motifs might differ in their ability to govern these two human transgenes. This might not be a valid assumption, however, because many transcription factors and their DNA-binding motifs are highly conserved among vertebrates and, indeed, in some cases down to the fly, worm and yeast.

The BAC carrying the human *CYP1A1_CYP1A2* locus includes the 23.3-kb bidirectional promoter, plus 56 kb 3′-ward of *CYP1A1* and 86 kb 3′-ward of *CYP1A2* (Jiang et al., 2005). The transgenes in the *hCYP1A1_1A2_Cyp1a1/1a2(−/−)* mouse thus would carry human *cis*-regulatory motifs only within these sequences responsible for TCDD up-regulation, whereas expression of the human *CYP1A1* and *CYP1A2* genes in chimeric mice should be controlled by any and all of the human *cis*- and *trans*-regulatory enhancers in the same way as they are in human liver hepatocytes.

The expression level of mouse CYP1A1 induced mRNA in B6 is comparable to that in *uPA/SCID* mice and might also be comparable to that in chimeric mice when the human hepatocyte-replacement rate is taken into consideration. A similar conclusion might also be reached if one compares the expression levels of mouse induced CYP1A2 mRNA among B6, chimeric, and *uPA/SCID* mice. As a whole, we conclude that the *hCYP1A1_1A2_Cyp1a1/1a2(−/−)* line and the human hepatocyte chimeric mouse show similar expression levels of basal mRNA for the human *CYP1A1* and *CYP1A2* genes. Likewise, there are similar expression levels of TCDD-induced mRNA for these two genes, although their extent of induction is variable.

Comparison of human versus mouse CYP1A1 and CYP1A2 protein levels in liver

Western immunoblots of liver were carried out from the four mouse types, control versus TCDD-pretreated (Fig. 2). The polyvalent antiserum was raised against rat CYP1A1/1A2 and thus is not likely to recognize equally the human and mouse CYP1A1 and CYP1A2 proteins; consequently, a strict quantitative comparison of the human versus mouse orthologous protein concentrations is not possible. This problem has been recognized before and discussed in detail (Jiang et al., 2005).

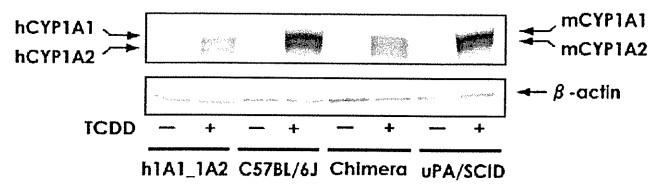

Fig. 2. Western immunoblot analysis of mouse versus human hepatic CYP1A1 and CYP1A2 proteins in the same mouse lines as in Fig. 1, using a polyclonal antibody that recognizes both mammalian CYP1A1 and CYP1A2. TCDD-induced mouse and human CYP1A1 proteins are both ~56.0 kDa, whereas TCDD-induced mouse and human CYP1A2 proteins are both ~54.5 kDa. Lanes 1–2 represent human CYP1A proteins only, whereas lanes 5–6 represent ~78% human CYP1A proteins and ~22% mouse CYP1A proteins. Lanes 3–4 and 7–8 depict only mouse CYP1A proteins. We used β-actin mRNA as a control for standardizing the amount of protein loaded per lane. The amount of microsomal protein (10 µg) loaded per lane was constant for all lanes.

Comparison of human versus mouse CYP1A1 and CYP1A2 TCDD-induced enzyme activities in liver

For BaP hydroxylase and EROD as two activities associated predominantly with CYP1A1, the correlations between enzyme activities (Fig. 3A) and mRNA levels (Fig. 1A) are extremely variable for BaP hydroxylase but quite consistent for EROD activity. Thus, B6 mice exhibit one-half as much TCDD-induced BaP hydroxylase activity (per unit of mCYP1A1 mRNA) as *uPA/SCID* mice (Table 2). The B6 mouse shows ~170 times more induced BaP hydroxylase activity (per unit of mCYP1A1 mRNA), compared with the *hCYP1A1_1A2_Cyp1a1/1a2(−/−)* mouse's induced BaP hydroxylase activity (per unit of hCYP1A1 mRNA). Chimeric mice exhibit ~6.2-fold more induced BaP hydroxylase activity (per unit of hCYP1A1 mRNA) than *hCYP1A1_1A2_Cyp1a1/1a2(−/−)* mice (Table 2). The *uPA/SCID* mouse shows ~42 times more induced BaP hydroxylase activity (per unit of mCYP1A1 mRNA), compared with the chimeric mouse's induced BaP hydroxylase activity (per unit of hCYP1A1 mRNA).

In contrast, B6 mice display about the same amount of TCDD-induced EROD activity (per unit of mCYP1A1 mRNA) as *uPA/SCID* mice (Table 2). The B6 mouse shows ~54 times more induced EROD activity (per unit of mCYP1A1 mRNA), compared with the *hCYP1A1_1A2_Cyp1a1/1a2(−/−)* mouse's induced EROD activity (per unit of hCYP1A1 mRNA). Chimeric mice exhibit ~1.7 times more induced EROD activity (per unit of hCYP1A1 mRNA) than *hCYP1A1_1A2_Cyp1a1/1a2(−/−)* mice (Table 2). The *uPA/SCID* mouse shows ~39 times more induced EROD activity (per unit of mCYP1A1 mRNA), compared with the chimeric mouse's induced EROD activity (per unit of hCYP1A1 mRNA).

Why does the humanized *hCYP1A1_1A2_Cyp1a1/1a2(−/−)* mouse carry so little enzyme activity toward BaP, compared with the chimeric mouse? This difference can be explained from the human hepatocyte-replacement rate (73%–83%) in chimeric mice. The liver of chimeric mice carries 73%–83% human hepatocytes, which exhibit extremely low BaP hydroxylase activity.

For acetanilide 4-hydroxylase and MROD as two activities associated predominantly with CYP1A2, the correlations between enzyme activities (Fig. 3B) and mRNA levels (Fig. 1B) are very much consistent with one another. B6 mice show virtually the same amount of TCDD-induced acetanilide 4-hydroxylase activity (per unit of mCYP1A2 mRNA) as *uPA/SCID* mice (Table 2). The B6 mouse shows about the same amount of induced acetanilide 4-hydroxylase activity (per unit of mCYP1A2 mRNA), compared with the *hCYP1A1_1A2_Cyp1a1/1a2(−/−)* mouse's induced acetanilide 4-hydroxylase activity (per unit of hCYP1A2 mRNA). Chimeric mice exhibit twice as much induced acetanilide 4-hydroxylase activity (per unit of hCYP1A2 mRNA) than *hCYP1A1_1A2_Cyp1a1/1a2(−/−)* mice (Table 2). The chimeric mouse shows ~2.3-fold more induced acetanilide 4-hydroxylase activity (per unit of mCYP1A2 mRNA), compared with the *uPA/SCID* mouse's induced acetanilide 4-hydroxylase activity (per unit of hCYP1A2 mRNA).

B6 mice exhibit one-half as much TCDD-induced MROD activity (per unit of mCYP1A2 mRNA) as *uPA/SCID* mice (Table 2). The *hCYP1A1_1A2_Cyp1a1/1a2(−/−)* mouse shows ~2-fold more induced MROD activity (per unit of mCYP1A2 mRNA), compared with the B6 mouse's induced MROD activity (per unit of hCYP1A2 mRNA). The *hCYP1A1_1A2_Cyp1a1/1a2(−/−)* mice exhibit ~2.4 times more in-

Table 2
Ratios of mouse liver TCDD-induced enzymic activities per unit of mRNA*.

	mCYP1A1		hCYP1A1	
B6 mouse	7600 ± 2700	h1A1_1A2	44 ± 13	BaP hydroxylase
uPA/SCID	11,400 ± 3000	Chimera	270 ± 62	
B6 mouse	230 ± 64	h1A1_1A2	4.3 ± 1.3	EROD activity
uPA/SCID	290 ± 95	Chimera	7.4 ± 3.1	
	mCYP1A2		hCYP1A2	
B6 mouse	490 ± 84	h1A1_1A2	600 ± 220	Acetanilide
uPA/SCID	510 ± 200	Chimera	1200 ± 390	4-hydroxylase
B6 mouse	5.4 ± 1.0	h1A1_1A2	14 ± 5.5	MROD activity
uPA/SCID	13 ± 5.2	Chimera	5.6 ± 0.3	

* For BaP hydroxylase, these ratios represent FU/min/mg protein divided by mRNA × 10^6 per μg total RNA. For the other three enzyme activities, these ratios represent pmol/min/mg protein divided by mRNA × 10^9 per μg total RNA. Values are expressed as means ± S.E.

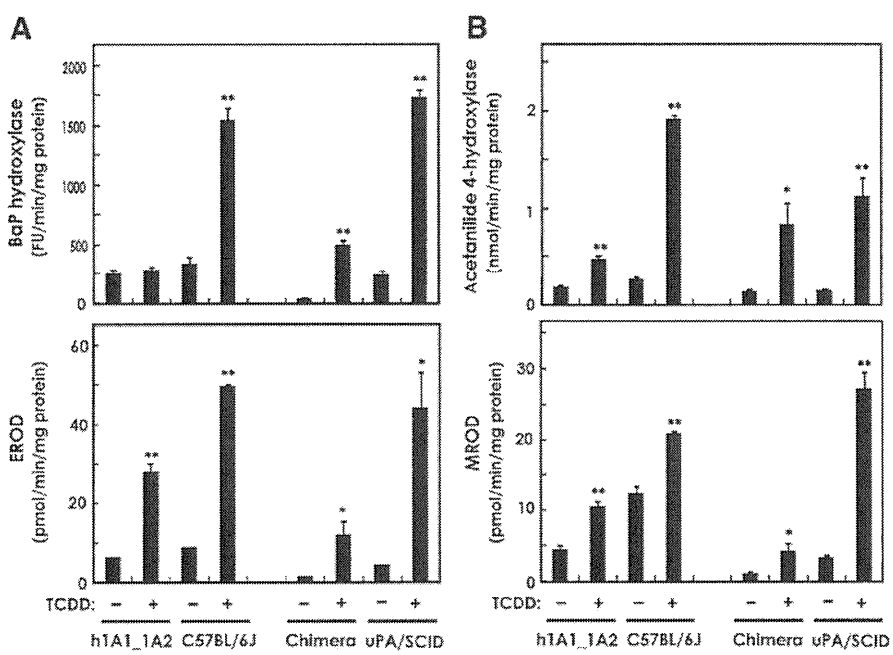

Fig. 3. (A) BaP hydroxylase and EROD activity (both representing largely CYP1A1), and (B) acetanilide 4-hydroxylase and MROD activity (both representing largely CYP1A2) in liver microsomes from the same mouse lines as in Fig. 1. FU, fluorescent units. *$P < 0.05$ and **$P < 0.01$, when comparing TCDD-pretreated with no pretreatment.

duced MROD activity (per unit of hCYP1A2 mRNA) than chimeric mice (Table 2). The *uPA/SCID* mouse shows twice as much induced MROD activity (per unit of mCYP1A2 mRNA), compared with the chimeric mouse's induced MROD activity (per unit of hCYP1A2 mRNA). Expression of CYP1A2 catalytic activity, relative to CYP1A2 mRNA levels, in the humanized *hCYP1A1_1A2_Cyp1a1/1a2(−/−)* and chimeric mouse lines is therefore very robust and within 2-fold similar to that expressed in mouse liver.

Comparison of human versus mouse CYP1A1 and CYP1A2 mRNA levels in hepatoma-derived cell culture lines

Animal rights' activists have urged scientists to study physiological functions in cell cultures rather than using live laboratory animals. Many studies have shown, however, that parameters found in cell culture do not accurately reflect what happens in the intact animal.

How does the expression of the *CYP1A1* and *CYP1A2* genes in intact liver compare with that in hepatoma-derived established cell lines? In HepG2 cells (Fig. 4A), human basal CYP1A1 mRNA was negligible, whereas human TCDD-induced CYP1A1 mRNA gave ~5.4×10^9 copy numbers (per μg total RNA). In Hepa-1c1c7 cells (Fig. 4A), mouse basal versus TCDD-induced CYP1A1 mRNA showed ~0.35×10^8 and ~1.9×10^8 copy numbers, respectively. Mouse CYP1A1 mRNA was not detected in HepG2, and human CYP1A1 mRNA was not detected in Hepa-1c1c7 cells.

In HepG2 cells (Fig. 4B), human basal versus TCDD-induced CYP1A2 mRNA gave ~0.27×10^6 and ~4.8×10^6 copy numbers, respectively. In Hepa-1c1c7 cells (Fig. 4B), mouse basal versus TCDD-induced CYP1A2 mRNA showed ~0.14×10^6 and ~1.2×10^6 copies, respectively. Mouse CYP1A2 mRNA was not detected in HepG2, and human CYP1A2 mRNA was not detected in Hepa-1c1c7 cells.

Thus, in livers of the *hCYP1A1_1A2_Cyp1a1/1a2(−/−)* and chimeric mice, the copy number of human induced CYP1A1 mRNA is 7.5 and 2.6 times, respectively, greater than that of human induced CYP1A2 mRNA. On the other hand, in the HepG2 liver-derived established cell line, the copy number of human induced CYP1A1 mRNA is more than 1100 times greater than that of human induced CYP1A2 mRNA. In livers of the B6 and *uPA/SCID* mice, the copy number of mouse induced CYP1A2 mRNA is 40-fold and 20-fold, respectively, greater than that of mouse induced CYP1A1 mRNA; in contrast, in the Hepa-1c1c7 established cell line, the copy number of mouse induced CYP1A1 mRNA is almost 1600-fold greater than that of mouse maximally-inducible CYP1A2 mRNA. This decline in *CYP1A2* gene expression seen in established cell lines reflects the well-known fact that numerous "housekeeping" genes such as *CYP1A2* are extinguished, or are greatly decreased in expression—in tumor cells as well as "established", or transformed, cell lines in culture (Owens et al., 1975; Nebert, 2006). However, such suppression often does not occur for the *CYP1A1* gene in differentiated tumors, including the HepG2 and Hepa-1c1c7 hepatoma-derived cell lines (Owens et al., 1975; Nebert, 2006).

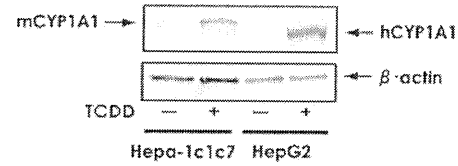

Fig. 5. Western immunoblot analysis of mouse versus human hepatic CYP1A1 and CYP1A2 proteins in the same cell culture lines as in Fig. 4. Everything is the same as that described for the Western blot in Fig. 2. The amount of cell culture protein (10 μg) loaded per lane was constant for all lanes.

Comparison of human versus mouse CYP1A1 and CYP1A2 protein levels in hepatoma-derived cell culture lines

We carried out Western immunoblots of Hepa-1c1c7 and HepG2 cells, control versus TCDD-pretreated (Fig. 5). The human CYP1A1 protein appears to migrate more rapidly than the mouse CYP1A1 protein. We believe the level of CYP1A2 protein was so low that it was not detected in either established hepatoma cell line.

Comparison of human versus mouse CYP1A1 and CYP1A2 TCDD-induced enzyme activities in hepatoma-derived cell culture lines

Different from what was found in mouse liver, the correlations between enzyme activities (Fig. 6A) and mRNA levels (Fig. 4A) are extremely variable for EROD activity but more consistent for BaP

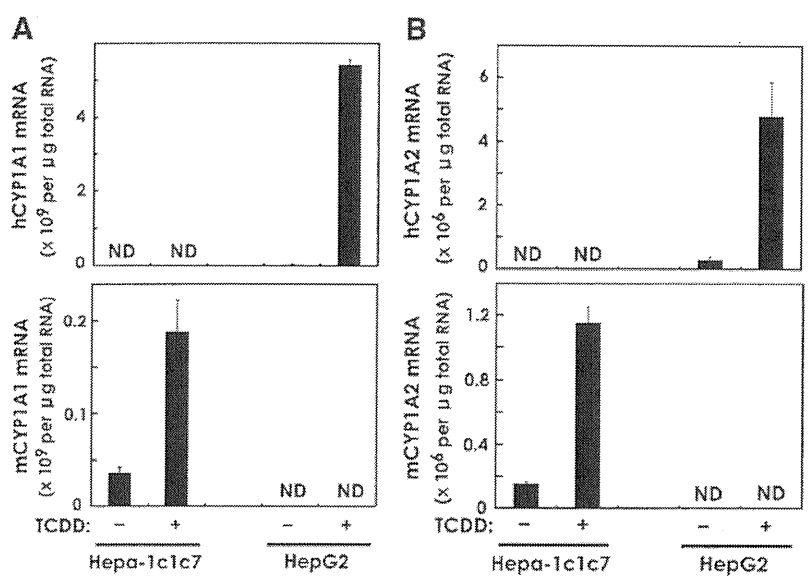

Fig. 4. Human (*upper panels*) versus mouse (*lower panels*) CYP1A1 (A) and CYP1A2 (B) mRNA copy numbers in mouse Hepa-1c1c7 cells and human HepG2 cells—with, versus without, TCDD exposure (10 nM for 24 h) in culture. Abbreviations are the same as those in Fig. 1.

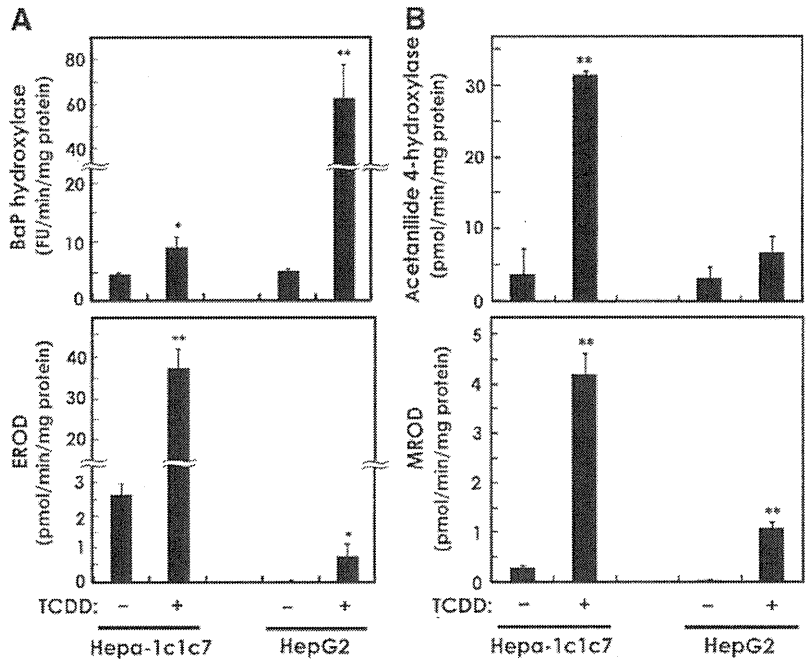

Fig. 6. (A) BaP hydroxylase and EROD activity (both representing largely CYP1A1), and (B) acetanilide 4-hydroxylase and MROD activity (both representing largely CYP1A2) in the same cell culture lines as in Fig. 4. $^{*}P<0.05$ and $^{**}P<0.01$, when comparing TCDD-pretreated with no pretreatment.

hydroxylase activity. Hepa-1c1c7 cells show ~4.8 times more TCDD-induced BaP hydroxylase activity (per unit of mCYP1A1 mRNA) than HepG2 cells exhibit for induced BaP hydroxylase activity (per unit of hCYP1A1 mRNA) (Table 3). Hepa-1c1c7 cells show ~1500 times more TCDD-induced EROD activity (per unit of mCYP1A1 mRNA) than HepG2 cells exhibit for induced EROD activity (per unit of hCYP1A1 mRNA). For whatever reason, HepG2 cells do not display very high induced BaP hydroxylase activity, and their induced EROD activity is extremely low.

For acetanilide 4-hydroxylase and MROD as two activities associated predominantly with CYP1A2, the correlations between enzyme activities (Fig. 6B) and mRNA levels (Fig. 6B) are better than those with CYP1A1. Hepa-1c1c7 cells show ~16-fold more TCDD-induced acetanilide 4-hydroxylase activity (per unit of mCYP1A2 mRNA) than HepG2 cells exhibit for induced acetanilide 4-hydroxylase activity (per unit of hCYP1A2 mRNA) (Table 3). Hepa-1c1c7 cells show ~15-fold more TCDD-induced MROD activity (per unit of mCYP1A2 mRNA) than HepG2 cells exhibit for induced MROD activity (per unit of hCYP1A2 mRNA). Therefore, HepG2 cells do not express either CYP1A1 or CYP1A2 activities nearly as robustly as do Hepa-1c1c7 cells.

Table 3
Ratios of hepatoma-derived cell line TCDD-induced enzymic activities per unit of mRNA*.

	mCYP1A1		hCYP1A1	
Hepa-1c1c7	55 ± 21	HepG2	11 ± 2.5	BaP hydroxylase
Hepa-1c1c7	210 ± 48	HepG2	0.14 ± 0.06	EROD activity
	mCYP1A2		**hCYP1A2**	
Hepa-1c1c7	27,000 ± 2400	HepG2	1800 ± 930	Acetanilide 4-hydroxylase
Hepa-1c1c7	3700 ± 480	HepG2	250 ± 85	MROD activity

* For BaP hydroxylase, these ratios represent FU/min/mg protein divided by mRNA × 10^9 per μg total RNA. For the other three enzyme activities, these ratios represent pmol/min/mg protein divided by mRNA × 10^9 per μg total RNA. Values are expressed as means ± S.E.

Conclusions

In this study we have measured the amount of variability between human and mouse CYP1A mRNA and protein levels and corresponding enzyme activities in the humanized *hCYP1A1_1A2_Cyp1a1/1a2(−/−)* and chimeric *uPA/SCID* lines, by comparing these parameters with those seen in wild-type mice from which these two lines were derived. We have also compared these mRNA and protein levels and corresponding enzyme activities in mouse hepatoma-derived Hepa-1c1c7 and human hepatoblastoma-derived HepG2 established cell culture lines. Clearly, the CYP1A1/CYP1A2 activity ratios in these hepatoma-derived established cell lines are not accurate indicators of those in liver from the intact mouse. Undoubtedly, this discrepancy is primarily caused by the dramatically lowered CYP1A2 mRNA levels—presumably due to "extinction" of the normal expression of the *CYP1A2* gene in these hepatoma-derived established cell lines. Not only very low CYP1A2 enzyme activity per unit of mRNA was seen in both Hepa-1c1c7 and HepG2 cells, but also low CYP1A1 enzyme activity per unit of hCYP1A1 mRNA was found in HepG2 cells.

Comparing liver of the two humanized mouse lines with liver of mice from which these two humanized lines were derived was most disturbing when one examined CYP1A1-specific (BaP and ethoxyresorufin) and CYP1A2-specific (acetanilide and methoxyresorufin) substrates metabolized—per unit of mCYP1A1, hCYP1A1, mCYP1A2 or hCYP1A2 mRNA. The hCYP1A1 in mouse liver was between 38 and more than 170 times less efficient than mCYP1A1 in the hydroxylation of BaP and about 54-fold less efficient in EROD activity. In contrast, hCYP1A2 in mouse liver appeared to function nearly equivalent to mCYP1A2 in wild-type mouse liver.

The levels of human CYP1A1 and CYP1A2 mRNA in both humanized mouse lines appear to be quite compatible with what might be expected among individual persons in any human population. It is very clear, however, that substrate specificity varies widely, independent of human versus mouse CYP1A1/1A2 mRNA or protein concentrations. Nevertheless, keeping this caveats in mind, both of these lines should still be useful for studies in human risk assessment, toxicology, pharmacology, and other medical subspecialties.

Note added in proof

A recent study (Wilson et al., 2008) is directly relevant to the problems addressed in our present manuscript. This study involves Tc1 hepatocytes, derived from an aneuploid mouse strain carrying human chromosome (Chr) 21 in addition to the entire mouse genome. The authors compared the regulation of human genes in Tc1 cells to that of the mouse orthologous genes in these same cells, using mouse wild-type versus human wild-type cells as controls. Regulation in the nuclei of Tc1 cells was compared at three levels: binding of transcription factors to DNA, modification of histones, and gene expression. The binding patterns of HNF1α, HNF4α and HNF6 on human Chr 21 in Tc1 cells matched closely those seen in human wild-type cells, rather than those seen in mouse wild-type cells. Similarly, histone modifications–as well as gene expression (the amount of mRNA transcribed)–showed human-specific, instead of mouse-specific, patterns on human Chr 21 in Tc1 cells. The authors concluded that it is the regulatory DNA sequence, rather than any other species-specific factor, which is the single most important determinant of gene expression (Wilson et al., 2008).

Acknowledgments

We thank our colleagues for many fruitful discussions and careful readings of this manuscript. Supported, in part, by the Ministry of Education, Science, Sports & Culture, Japan (Grant-in-Aid for Scientific Research on Priority Areas, 18077005 to S.U. and M.M.), and Nihon University Joint Research Grant for 2007 (S.U.), and NIH Grants R01 ES014403 (D.W.N.) and P30 ES06096 (D.W.N.).

References

Aoyama, T., Gonzalez, F.J., Gelboin, H.V., 1989. Human cDNA-expressed cytochrome P450 1A2: mutagen activation and substrate specificity. Mol. Carcinog. 2, 192–198.

Bedell, M.A., Jenkins, N.A., Copeland, N.G., 1996. Good genes in bad neighbourhoods. Nat. Genet. 12, 229–232.

Bennett, L.M., McAllister, K.A., Blackshear, P.E., Malphurs, J., Goulding, G., Collins, N.K., Ward, T., Bunch, D.O., Eddy, E.M., Davis, B.J., Wiseman, R.W., 2000. *Brca2*-null embryonic survival is prolonged on the BALB/c genetic background. Mol. Carcinog. 28, 174–183.

Bernhard, H.P., Darlington, G.J., Ruddle, F.H., 1973. Expression of liver phenotypes in cultured mouse hepatoma cells: synthesis and secretion of serum albumin. Dev. Biol. 35, 83–96.

Berthou, F., Guillois, B., Riche, C., Dreano, Y., Jacqz-Aigrain, E., Beaune, P.H., 1992. Interspecies variations in caffeine metabolism related to cytochrome P450 1A enzymes. Xenobiotica 22, 671–680.

Bonyadi, M., Rusholme, S.A., Cousins, F.M., Su, H.C., Biron, C.A., Farrall, M., Akhurst, R.J., 1997. Mapping of a major genetic modifier of embryonic lethality in *Tgfb1(−/−)* knockout mice. Nat. Genet. 15, 207–211.

Burke, M.D., Mayer, R.T., Kouri, R.E., 1977. 3-Methylcholanthrene-induced monooxygenase (*O*-deethylation) activity of human lymphocytes. Cancer Res. 37, 460–463.

Cheung, C., Ma, X., Krausz, K.W., Kimura, S., Feigenbaum, L., Dalton, T.P., Nebert, D.W., Idle, J.R., Gonzalez, F.J., 2005. Differential metabolism of 2-amino-1-methyl-6-phenylimidazo[4,5-*b*]pyridine (PhIP) in mice humanized for CYP1A1 and CYP1A2. Chem. Res. Toxicol. 18, 1471–1478.

Cranston, A., Fishel, R., 1999. Female embryonic lethality in *Msh2–Trp53* nullizygous mice is strain-dependent. Mamm. Genome 10, 1020–1022.

Dalton, T.P., Dieter, M.Z., Matlib, R.S., Childs, N.L., Shertzer, H.G., Genter, M.B., Nebert, D.W., 2000. Targeted knockout of *Cyp1a1* gene does not alter hepatic constitutive expression of other genes in the mouse [*Ah*] battery. Biochem. Biophys. Res. Commun. 267, 184–189.

Dearfield, K.L., Jacobson-Kram, D., Brown, N.A., Williams, J.R., 1983. Evaluation of a human hepatoma cell line as a target cell in genetic toxicology. Mutat. Res. 108, 437–449.

Derkenne, S., Curran, C.P., Shertzer, H.G., Dalton, T.P., Dragin, N., Nebert, D.W., 2005. Theophylline pharmacokinetics: comparison of *Cyp1a1(−/−)* and *Cyp1a2(−/−)* knockout mice, humanized *hCYP1A1_1A2* knock-in mice lacking either the mouse *Cyp1a1* or *Cyp1a2* gene, and *Cyp1(+/+)* wild-type mice. Pharmacogenet. Genomics 15, 503–511.

Dragin, N., Uno, S., Wang, B., Dalton, T.P., Nebert, D.W., 2007. Generation of 'humanized' *hCYP1A1_1A2_Cyp1a1/1a2(−/−)* mouse line. Biochem. Biophys. Res. Commun. 359, 635–642.

Eaton, D.L., Gallagher, E.P., Bammler, T.K., Kunze, K.L., 1995. Role of cytochrome P450 1A2 in chemical carcinogenesis: implications for human variability in expression and enzyme activity. Pharmacogenetics 5, 259–274.

Giannini, C., Morosan, S., Tralhao, J.G., Guidotti, J.E., Battaglia, S., Mollier, K., Hannoun, L., Kremsdorf, D., Gilgenkrantz, H., Charneau, P., 2003. A highly efficient, stable, and rapid approach for ex vivo human liver gene therapy via a FLAP lentiviral vector. Hepatology 38, 114–122.

Hamm, J.T., Ross, D.G., Richardson, V.M., Diliberto, J.J., Birnbaum, L.S., 1998. Methoxyresorufin: an inappropriate substrate for CYP1A2 in the mouse. Biochem. Pharmacol. 56, 1657–1660.

Inaba, Y., Yamamoto, K., Yoshimoto, N., Matsunawa, M., Uno, S., Yamada, S., Makishima, M., 2007. Vitamin D3 derivatives with adamantane or lactone ring side chains are cell type-selective vitamin D receptor modulators. Mol. Pharmacol. 71, 1298–1311.

Jiang, Z., Dalton, T.P., Jin, L., Wang, B., Tsuneoka, Y., Shertzer, H.G., Deka, R., Nebert, D.W., 2005. Toward the evaluation of function in genetic variability: characterizing human SNP frequencies and establishing BAC-transgenic mice carrying the human *CYP1A1_CYP1A2* locus. Hum. Mutat. 25, 196–206.

Katoh, M., Tateno, C., Yoshizato, K., Yokoi, T., 2008. Chimeric mice with humanized liver. Toxicology 246, 9–17.

Lindberg, R.L., Negishi, M., 1989. Alteration of mouse cytochrome P450coh substrate specificity by mutation of a single amino-acid residue. Nature 339, 632–634.

Milot, E., Fraser, P., Grosveld, F., 1996. Position effects and genetic disease. Trends Genet. 12, 123–126.

Muller, K., Heller, H., Doerfler, W., 2001. Foreign DNA integration. Genome-wide perturbations of methylation and transcription in the recipient genomes. J. Biol. Chem. 276, 14271–14278.

Nebert, D.W., 1989. The *Ah* locus: genetic differences in toxicity, cancer, mutation, and birth defects. Crit. Rev. Toxicol. 20, 153–174.

Nebert, D.W., 2006. Comparison of gene expression in cell culture to that in the intact animal: relevance to drugs and environmental toxicants. Am. J. Physiol., Cell Physiol. 290, C37–C41.

Nebert, D.W., Dalton, T.P., 2006. The role of cytochrome P450 enzymes in endogenous signalling pathways and environmental carcinogenesis. Nat. Rev., Cancer 6, 947–960.

Nebert, D.W., Gelboin, H.V., 1968. Substrate-inducible microsomal aryl hydroxylase in mammalian cell culture. I. Assay and properties of induced enzyme. J. Biol. Chem. 243, 6242–6249.

Nebert, D.W., Dalton, T.P., Okey, A.B., Gonzalez, F.J., 2004. Role of aryl hydrocarbon receptor-mediated induction of the CYP1 enzymes in environmental toxicity and cancer. J. Biol. Chem. 279, 23847–23850.

Nelson, D.R., Koymans, L., Kamataki, T., Stegeman, J.J., Feyereisen, R., Waxman, D.J., Waterman, M.R., Gotoh, O., Coon, M.J., Estabrook, R.W., Gunsalus, I.C., Nebert, D.W., 1996. P450 superfamily: update on new sequences, gene mapping, accession numbers and nomenclature. Pharmacogenetics 6, 1–42.

Nelson, D.R., Zeldin, D.C., Hoffman, S.M., Maltais, L.J., Wain, H.M., Nebert, D.W., 2004. Comparison of cytochrome P450 (*CYP*) genes from the mouse and human genomes, including nomenclature recommendations for genes, pseudogenes, and alternative-splice variants. Pharmacogenetics 14, 1–18.

Nichols, R.C., Cooper, S., Trask, H.W., Gorman, N., Dalton, T.P., Nebert, D.W., Sinclair, J.F., Sinclair, P.R., 2003. Uroporphyrin accumulation in hepatoma cells expressing human or mouse CYP1A2: relation to the role of CYP1A2 in human porphyria cutanea tarda. Biochem. Pharmacol. 65, 545–550.

Olson, E.N., Arnold, H.H., Rigby, P.W., Wold, B.J., 1996. Know your neighbors: three phenotypes in null mutants of the myogenic bHLH gene *Mrf4*. Cell 85, 1–4.

Owens, I.S., Niwa, A., Nebert, D.W., 1975. In: Gerschenson, L.E., Thompson, E.B. (Eds.), Expression of Aryl Hydrocarbon Hydroxylase Induction in Liver- and Hepatoma-Derived Cell Cultures. Academic Press, New York, NY, pp. 378–401.

Shertzer, H.G., Nebert, D.W., Senft, A.P., Dingledein, M., Genter, M.B., Dalton, T.P., 2001. Spectrophotometric assay for acetanilide 4-hydroxylase, an estimate of CYP1A2 enzyme activity. Toxicol. Meth. 11, 81–88.

Shi, Z., Chen, Y., Dong, H., Amos-Kroohs, R.M., Nebert, D.W., 2008. Generation of 'humanized' *hCYP1A1_1A2_Cyp1a1/1a2(−/−)_Ahr*^{d} mouse line harboring the poor-affinity aryl hydrocarbon receptor. Biochem. Biophys. Res. Commun. 376, 775–780.

Tateno, C., Yoshizane, Y., Saito, N., Kataoka, M., Utoh, R., Yamasaki, C., Tachibana, A., Soeno, Y., Asahina, K., Hino, H., Asahara, T., Yokoi, T., Furukawa, T., Yoshizato, K., 2004. Near completely humanized liver in mice shows human-type metabolic responses to drugs. Am. J. Pathol. 165, 901–912.

Tavangar, K., Hoffman, A.R., Kraemer, F.B., 1990. A micromethod for the isolation of total RNA from adipose tissue. Anal. Biochem. 186, 60–63.

Turesky, R.J., 2005. Interspecies metabolism of heterocyclic aromatic amines and the uncertainties in extrapolation of animal toxicity data for human risk assessment. Mol. Nutr. Food Res. 49, 101–117.

Uno, S., Dalton, T.P., Dragin, N., Curran, C.P., Derkenne, S., Miller, M.L., Shertzer, H.G., Gonzalez, F.J., Nebert, D.W., 2006. Oral benzo[*a*]pyrene in *Cyp1* knockout mouse lines: CYP1A1 important in detoxication, CYP1B1 metabolism required for immune damage independent of total-body burden and clearance rate. Mol. Pharmacol. 69, 1103–1114.

Uno, S., Dragin, N., Miller, M.L., Dalton, T.P., Gonzalez, F.J., Nebert, D.W., 2008. Basal and inducible CYP1 mRNA quantitation and protein localization throughout the mouse gastrointestinal tract. Free Radic. Biol. Med. 44, 570–583.

Wilson, M.D., Barbosa-Morais, N.L., Schmidt, D., Conboy, C.M., Vanes, L., Tybulewicz, V.L., Fisher, E.M., Tavaré, S., Odom, D.T., 2008. Species-specific transcription in mice carrying human chromosome 21. Science 322, 434–438.

Winer, J., Jung, C.K., Shackel, I., Williams, P.M., 1999. Development and validation of real-time quantitative reverse transcriptase-polymerase chain reaction for monitoring gene expression in cardiac myocytes in vitro. Anal. Biochem. 270, 41–49.

Inhibition of Transforming Growth Factor β Signaling by Halofuginone as a Modality for Pancreas Fibrosis Prevention

Orit Zion, MSc, Olga Genin, MSc,* Norifumi Kawada, MD,† Katsutoshi Yoshizato, MD,‡ Suzy Roffe, MsC,§ Arnon Nagler, MD,|| Juan L. Iovanna, MD, PhD,¶ Orna Halevy, PhD,§ and Mark Pines, PhD**

Objectives: Chronic pancreatitis is characterized by inflammation and fibrosis. We evaluated the efficacy of halofuginone, an inhibitor of collagen synthesis and myofibroblast activation, in preventing cerulein-induced pancreas fibrosis.

Methods: Collagen synthesis was evaluated by in situ hybridization and staining. Levels of prolyl 4-hydroxylase β (P4Hβ), cytoglobin/stellate cell activation–associated protein (Cygb/STAP), transgelin, tissue inhibitors of metalloproteinases, serum response factor, transforming growth factor β (TGFβ), Smad3, and pancreatitis-associated protein I (PAP-I) were determined by immunohistochemistry. Metalloproteinase activity was evaluated by zymography.

Results: Halofuginone prevented cerulein-dependent increase in collagen synthesis, collagen cross-linking enzyme P4Hβ, Cygb/STAP, and tissue inhibitors of metalloproteinase 2. Halofuginone did not affect TGFβ levels in cerulein-treated mice but inhibited serum response factor synthesis and Smad3 phosphorylation. In culture, halofuginone inhibited pancreatic stellate cell (PSC) proliferation and TGFβ-dependent increase in Cygb/STAP and transgelin synthesis and metalloproteinase 2 activity. Halofuginone increased c-Jun N-terminal kinase phosphorylation in PSCs derived from cerulein-treated mice. Halofuginone prevented the increase in acinar cell proliferation and further increased the cerulein-dependent PAP-I synthesis.

Conclusions: Halofuginone inhibits Smad3 phosphorylation and increases c-Jun N-terminal kinase phosphorylation, leading to the inhibition of PSC activation and consequent prevention of fibrosis. Halofuginone increased the synthesis of PAP-I, which further reduces pancreas fibrosis. Thus, halofuginone might serve as a novel therapy for pancreas fibrosis.

Key Words: myofibroblasts, pancreatic stellate cells, Smad, collagen, transgelin, cytoglobin

(*Pancreas* 2009;38: 427–435)

Chronic pancreatitis is a progressive disease, characterized by inflammation, fibrosis, and atrophy of the gland tissue, which results in impaired exocrine and endocrine functions of the pancreas.[1] The cellular mechanisms governing pancreas fibrosis are shared among the various insults and, in many aspects, mirror the scarring and wound-healing processes of other tissues. Pancreas fibrosis, regardless of the cause, is characterized by an increase in extracellular matrix (ECM) constituents, although their relative distribution within the pancreas varies with the site and nature of the insult.[2] In the injured pancreas, the pancreatic stellate cells (PSCs) constitute the major source of ECM proteins.[3] These cells are usually quiescent, with a low proliferation rate; however, upon activation, they differentiate into myofibroblastlike cells with high proliferative capacity. The activated PSCs migrate to sites of tissue damage, where they synthesize ECM components to promote tissue repair.[4] The intracellular signaling mechanisms regulating PSC activation include the mitogen-activated protein kinase (MAPK) pathway, which plays a major role in ethanol- and acetaldehyde-dependent activation of PSC, phosphatidylinositol-3-kinase, and protein kinase C.[5]

The transition to the myofibroblastlike phenotype is associated with increased expression of specific smooth muscle genes such as α smooth muscle actin and transgelin (SM22α) and of specific markers such as cytoglobin/stellate cell activation–associated protein (Cygb/STAP) in fibrotic lesions of the pancreas.[6] Pancreatic stellate cells can be activated directly by alcohol consumption[7] or by cytokines derived from the immigrating inflammatory cells.[8,9] Platelet-derived growth factor is the major promoter of PSC migration, whereas transforming growth factor β (TGFβ) affects ECM production via a Smad-associated pathway. Upon phosphorylation by the TGFβ receptor, Smad3 enters the nucleus to modulate the transcription of target genes.[10] Smad3 links TGFβ signaling directly to the serum response factor (SRF)–associated regulatory network that controls the expression of smooth muscle–specific genes.[11,12] The predominant ECM protein synthesized by the PSCs is collagen type I, although increases in the gene expression of other types of collagens and other matrix proteins have also been reported.[13] Pancreas fibrosis may also result from a relative imbalance between the production and degradation of matrix proteins.[14] The PSCs constitute the source of various matrix metalloproteinases (MMPs) and tissue inhibitors of MMPs (TIMPs), which are necessary for ECM remodeling under the control of TGFβ.[15,16]

In addition to the morbidity and mortality caused by chronic pancreatitis, patients with this disease also have a substantially increased risk of developing pancreatic cancer. The PSCs play a major role in the growth and development of pancreas adenocarcinoma, which has a remarkable fibrotic component regulated by the TGFβ pathway.[4,17,18] The desmoplasia is created by activated PSCs, which are stimulated by the cancer cells, thereby influencing tumor aggressiveness.[19] Given that activated PSCs not only are the principal effector cells in pancreas fibrosis but also play a major role in pancreas carcinoma, it seems that targeting the fibroblast-to-PSC transition might be a promising therapeutic approach, for which there is a great unmet need.

From the *Institute of Animal Sciences, The Volcani Center, Bet Dagan, Israel; †Department of Hepatology, Graduate School of Medicine, Osaka City University, Japan; ‡Developmental Biology Laboratory, CLUSTER Project, and 21st Century COE Program, Department of Biological Science, Graduate School of Science, Hiroshima University, Japan; §Department of Animal Sciences, The Hebrew University of Jerusalem, Rehovot, Israel; ||Department of Hematology and Bone Marrow Transplantation, Chaim Sheba Medical Center, Tel Hashomer, Israel; and ¶INSERM U624, Stress Cellulaire, Campus de Luminy, Marseille, France.

Received for publication July 23, 2008; accepted November 24, 2008.

Reprints: Mark Pines, PhD, Institute of Animal Science, ARO, The Volcani Center, Bet Dagan 50250, Israel (e-mail: pines@agri.huji.ac.il).

Halofuginone, an analog of the plant alkaloid febrifugine, has been found to inhibit the activation of hepatic stellate cells (HSCs)[20,21] and the stromal fibroblast-to-myofibroblast transition in the tumor microenvironment.[22] Halofuginone overcame TGFβ-induced collagen synthesis by inhibiting Smad3 phosphorylation downstream of the TGFβ signaling pathway.[23] In animal models in which excess collagen is the hallmark of the disease, halofuginone prevented the increase in collagen synthesis. These models included mice afflicted with chronic graft-versus-host disease and tight-skin mice, rats with pulmonary fibrosis, and rats that developed adhesions at various sites.[23–25] When given to rats that exhibited established fibrosis, halofuginone caused almost a complete resolution of the fibrotic condition.[20] In addition, halofuginone markedly improved the capacity of a cirrhotic liver to regenerate after partial hepatectomy[26] by affecting the expression of early genes of liver regeneration under the control of TGFβ.[27,28] Topical treatment with halofuginone of a patient with chronic graft-versus-host disease and of patients with scleroderma elicited a transient attenuation of collagen α_1(I) gene expression and improvements in skin scores, thus demonstrating human clinical efficacy.[25,29]

In the present study, we evaluated the efficacy of halofuginone in inhibiting pancreas fibrosis in mice, with particular emphasis on TGFβ-dependent PSC activation and ECM production.

MATERIALS AND METHODS

Materials

Halofuginone bromhydrate was obtained from Collgard Biopharmaceuticals Ltd (Tel Aviv, Israel). Cerulein and β-casein were from Sigma (St Louis, Mo). Antibodies to Cygb/STAP were prepared according to Nakatani et al.[6] Smad3 and phosphorylated Smad3 (P-Smad3) antibodies were from Abcam (Cambridge, United Kingdom). Serum response factor antibodies were from Santa Cruz Biotechnology Inc (Santa Cruz, Calif). The proliferating cell nuclear antigen (PCNA) staining kit was from Zymed Laboratories (San Francisco, Calif). Metalloproteinase 2 and P4Hβ monoclonal antibodies were from Acris (Hiddenhausen, Germany), and TIMP1 and TIMP2 monoclonal antibodies were from Lab Vision (Fremont, Calif). Polyclonal antibodies to phospho-Akt (S^{473}P-AKT), phospho-ERK/MAPK (P-p44), total Akt and total ERK/MAPK (p44), and monoclonal antibody to total c-Jun N-terminal kinase (JNK) 1 were from Cell Signaling Technologies (Danvers, Mass). Active-JNK (P-JNK1) and active p38 (P-p38) antibodies were from Promega (Madison, Wis). Rabbit polyclonal antibodies against human pancreatitis-associated protein 1 (PAP-1) were prepared as described previously.[30]

Animal Model of Pancreas Fibrosis

Male ICR mice (Harlan Laboratories, Jerusalem, Israel) were kept under standard conditions with free access to water and chow. Fibrosis was induced in mice (n = 10) by repeated (every 6 h) intraperitoneal injections of cerulein (50 μg/kg) twice weekly for 4 or 8 weeks according to Neuschwander-Tetri et al.[31] Halofuginone was administered intraperitoneally to mice (n = 10) at 4 μg per animal, 3 times per week as described by Bruck et al,[20] starting at the same time as the cerulein. Untreated mice (n = 10) and mice treated only with halofuginone (n = 10) were used as controls. All animal experiments were carried out according to the guidelines of the Volcani Center Institutional Committee for Care and Use of Laboratory Animals (Bet Dagan, Israel).

Preparation of Sections, In Situ Hybridization, and Immunohistochemistry

Pancreas samples were fixed overnight in 4% paraformaldehyde in phosphate-buffered saline at 4°C. Serial 5-μm sections were prepared after the samples had been embedded in Paraplast (McCormick Scientific, St Louis, Mo). Collagenous and noncollagenous proteins were differentially stained with 0.1% Sirius red and 0.1% Fast green as a counterstain, in saturated picric acid. By this procedure, collagen is stained red. Collagen levels were quantified by image analysis (ImagePro; Media Cybernetics, Silver Spring, Md). At least 20 photographs were taken for each analysis per each treatment at each time point. The results were calculated as the red area divided by the total red and green area and presented as arbitrary units of the mean (SE). Special care was taken to exclude the blank areas, which probably represented artifacts. In situ hybridization with a digoxigenin-labeled collagen α_1(I) probe was performed as described by Bruck et al.[20] No signal was observed with the sense probe. For immunohistochemistry, the following antibodies were used: SRF (diluted 1:500), TGFβ1 (1:400), Cygb/STAP (1:700), Smad3 (1:200), P-Smad2/3 (1:700), P4Hβ (1:25), TIMP1 (1:50), TIMP2 (1:250), and PAP-1 (1:10). In all cases, at least 5 slides from all the animals within the group were evaluated blindly to the animal grouping.

Cell Culture

Pancreatic stellate cells were prepared from either control mice or mice treated with a single injection of cerulein (50 μg/kg). After 24 hours, the pancreas was excised, freed from fat and lymph nodes, and digested with collagenase IV (0.02%), and the resulting cell suspension was centrifuged at 1200*g* for 5 minutes. The cells were washed and resuspended in Dulbecco's modified essential medium (DMEM) containing 10% fetal bovine serum and antibiotics (100-U/mL penicillin, 100-mg/mL streptomycin) and plated on 6-well plates with the same medium.[32] No significant differences were observed in the cell yield between the control and cerulein-treated mice, and almost all the cells were stained positive for Cygb/STAP or SM22α. All of the cells were incubated at 37°C in a humidified atmosphere containing 5% carbon dioxide. The cells were incubated with serum-free DMEM for 6 hours and were then treated with fresh medium containing halofuginone (20 or 50 nmol/L), TGFβ (3 ng/mL), or both for an additional 24 hours. Cellular viability was determined by trypan blue exclusion. At the end of the incubation period, the cells were either counted directly with a cell counter (Coulter Electronics, Bath, United Kingdom) or resuspended in 500 μL of lysis buffer consisting of 1-mmol/L EDTA, 50-mmol/L Tris (pH, 7.5), 150-mmol/L NaCl, 10% glycerol, 1% Nonidet P40, and a 1:100 dilution of protease and phosphatase inhibitor cocktail (Sigma).

Western Blot

Protein lysate (30 μg) from either tissue or cells was electrophoresed on a 10% sodium dodecyl sulfate–polyacrylamide gel and transferred onto a nitrocellulose membrane. Nonspecific binding sites were blocked with 5% low-fat milk, and the membranes were incubated overnight with the appropriate antibodies for SM22α (1:5000), Cygb/STAP (1:1000), MMP-2 (1:200), phospho-Akt (1:1000), phosphor–ERK/MAPK (1:2000), total Akt and total ERK/MAPK (1:1500), active

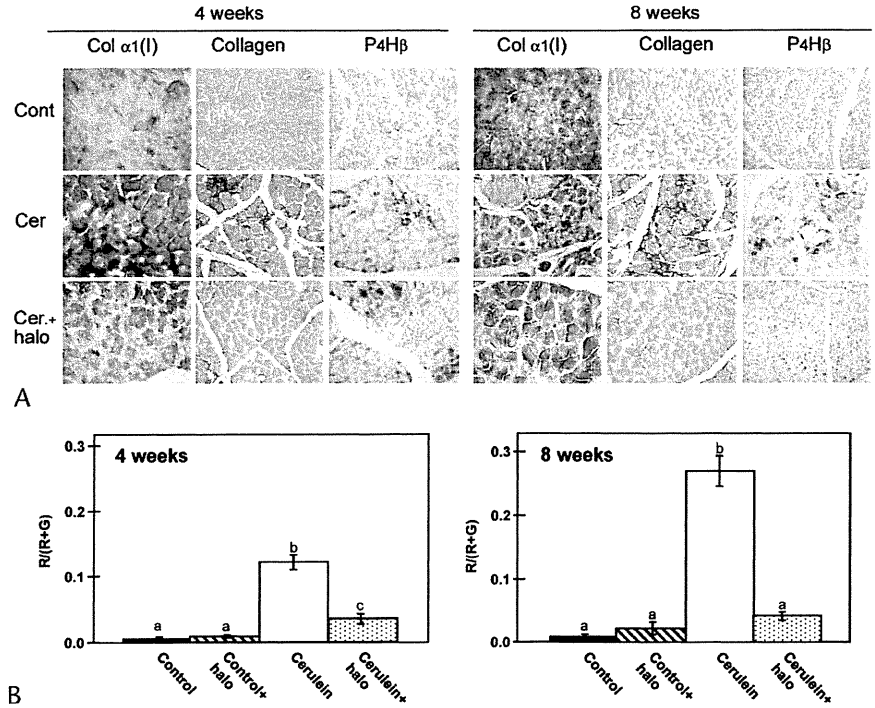

FIGURE 1. Effect of halofuginone on cerulein-dependent synthesis of collagen and P4Hβ, a collagen cross-linking enzyme. Mice were treated with cerulein for 4 or 8 weeks with or without halofuginone, after which pancreas biopsies were taken for histology. A, Collagen α_1(I) gene expression was determined by in situ hybridization, collagen level was evaluated by Sirius red staining, and P4Hβ was determined by immunohistochemistry. B, Image analysis of pancreas collagen levels. In each column, means without a common letter differ significantly ($P < 0.05$) according to Duncan multiple range test.

JNK (1:5000), active p38 (1:2000), and monoclonal antibody to total JNK (1:1000).

Zymography

Conditioned medium samples were analyzed for MMP activity, which was determined in a 10% sodium dodecyl sulfate–polyacrylamide gel impregnated with gelatin (0.01%) or β-casein (1.0 mg/mL). Proteins were separated on the gel under nonreducing conditions, followed by 1 hour of incubation in 2.5% Triton X-100 and 16 hours of incubation in 50-mmol/L Tris (pH, 7.6), 0.2-mol/L NaCl, and 5-mmol/L $CaCl_2$ at 37°C. After the incubation period, the gels were stained with 0.5% Coomassie G 250 in methanol/acetic acid/water (30:10:60, vol/vol/vol).

Statistical Analysis

The results are presented as the mean (SD). The significance of differences among different groups was determined by analysis of variance. In each column, means without a common letter differ significantly ($P < 0.05$) according to Duncan multiple range test.

RESULTS

Halofuginone Inhibits Pancreas Fibrosis

Pancreas fibrosis is the result of a dynamic cascade of mechanisms beginning with acinar cell injury and followed by inflammation and PSC activation. After 4 weeks of cerulein treatment, we observed a major increase in the number of PSCs expressing the collagen α_1(I) gene, the synthesis of large quantities of collagen surrounding the acinar cells, and positive staining for P4Hβ, one of the major enzymes responsible for collagen cross-linking and maturation (Fig. 1A). Collagen accumulated in the pancreas with time, and after an additional 4 weeks of cerulein treatment, a further increase in collagen content and P4Hβ level was observed. Halofuginone prevented the increase in fibrosis in a time-dependent fashion, as demonstrated by reductions in the expression of the collagen α_1(I) gene, in collagen content, and in the level of P4Hβ. After 4 weeks of halofuginone treatment, the collagen level was significantly lower than that of the cerulein-treated mice but was still higher than that of the control mice. After 8 weeks of halofuginone treatment, the collagen level was significantly lower than that of the cerulein-treated mice and did not differ from that of the control untreated mice (Fig. 1B). Halofuginone alone had no effect on the collagen content or other histologic parameters in the control untreated mice (data not shown).

Halofuginone Inhibits PSC Activation

In addition to enhancing collagen synthesis, activated PSCs are also characterized by increased proliferation and expression of SM22α and Cygb/STAP genes under the control of TGFβ. After 4 weeks of cerulein treatment, a major increase in the number of PSCs exhibiting Cygb/STAP was observed, which persisted for at least 8 weeks. Halofuginone reduced the number of Cygb/STAP-positive cells in the pancreas (Fig. 2A) and inhibited the TGFβ-induced Cygb/STAP levels in primary PSCs in cultures derived from the pancreas of control and cerulein-treated mice (Fig. 2B). Transgelin is induced during transdifferentiation of fibroblasts to myofibroblasts at the time of stromal tissue remodeling under the

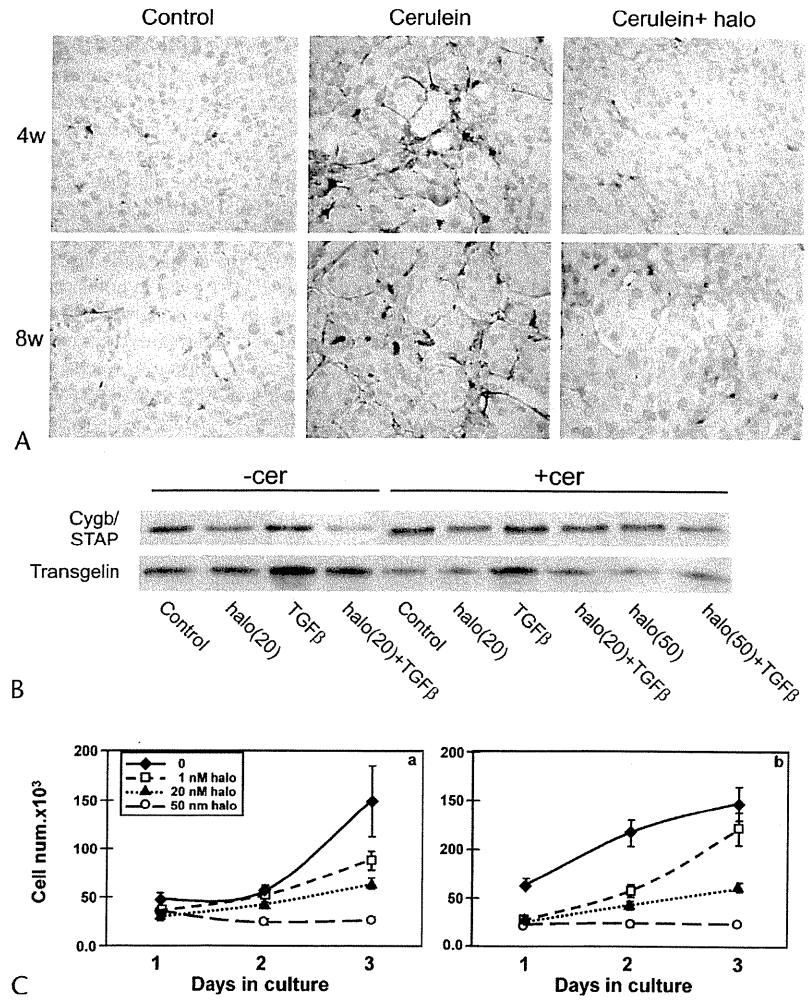

FIGURE 2. Effect of halofuginone on the synthesis of Cygb/STAP and SM22α and on PSC proliferation. A, Immunohistochemistry of Cygb/STAP in pancreas biopsies of mice treated for 4 or 8 weeks with cerulein, with or without halofuginone. B, Western blotting of Cygb/STAP and SM22α of PSCs derived from either control or cerulein-treated mice. The cells were incubated for 18 hours with TGFβ (3 ng/mL), halofuginone, or their combination. C, Primary PSCs were incubated with various concentrations of halofuginone, and cell proliferation was estimated directly by cell counting.

control of TGFβ. The PSCs in culture from control and cerulein-treated mice synthesized SM22α, which was upregulated by TGFβ. Halofuginone prevented the TGFβ-dependent SM22α synthesis in cultured primary PSCs derived from either control or cerulein-treated mice (Fig. 2B). The inhibitory effect of halofuginone on Cygb/STAP and SM22α synthesis was accompanied by a dose-dependent inhibition of proliferation of PSCs derived from either the normal pancreas or cerulein-treated mice (Fig. 2C). All of these findings were consistent with halofuginone inhibition of PSC activation.

Halofuginone and Matrix Degradation

The levels of TIMP1 and TIMP2 were increased in the pancreas after cerulein treatment, but only the TIMP2 level was inhibited by halofuginone (Fig. 3A). Metalloproteinase 2 is one of the major MMPs involved in pancreas fibrosis under the control of TGFβ.[14–16] Halofuginone had only a minimal, if any, effect on MMP-2 levels in the control mice. Cerulein treatment caused an increase in MMP-2 levels, which were further increased after halofuginone treatment (Fig. 3B). In culture, a major increase in basal MMP-2 activity was observed in conditioned medium of PSCs derived from cerulein-treated mice compared with controls (Fig. 3C). Halofuginone had no effect on the basal level of MMP-2 activity but inhibited the TGFβ-dependent increase in its activity by PSCs derived from control and cerulein-treated mice (Fig. 3D). In contrast, halofuginone increased MMP-3 activity, but only in PSCs derived from cerulein-treated mice (Fig. 3E).

Halofuginone Inhibits TGFβ Signaling

Almost no TGFβ was observed in the control untreated pancreas, whereas in the cerulein-treated mice, a major increase in its level was observed, mostly in the acinar cells but also in some of the PSCs (Fig. 4). Halofuginone treatment did not cause any change in the level of TGFβ, in agreement with previous studies suggesting that halofuginone affects TGFβ signaling downstream in its pathway.[23] Halofuginone treatment eliminated the synthesis of SRF, which was observed exclusively in the PSCs of the cerulein-treated pancreas. In the untreated pancreas, Smad3 was observed only in endothelial cells

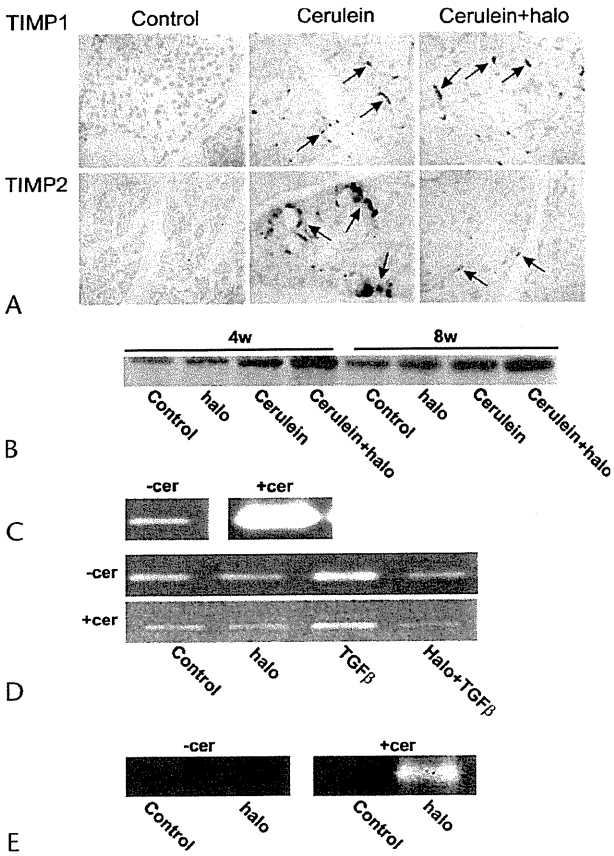

FIGURE 3. Halofuginone and the ECM degradation pathway. A, Immunohistochemistry of TIMP1 and TIMP2 in the pancreas after 8 weeks of cerulein treatment, with or without halofuginone. B, Western blotting with MMP-2 antibodies of pancreas extracts. C, Gelatin zymography for evaluation of MMP-2 activity in conditioned medium of PSCs derived from the cerulein-treated or untreated pancreas. Note the high levels of MMP-2 activity in conditioned medium of PSCs derived from the cerulein-treated pancreas. D, Effect of halofuginone on MMP-2 activity. E, Metalloproteinase 3 in conditioned medium collected from PSCs derived from the normal and the cerulein-treated pancreas.

surrounding the blood vessels, and no P-Smad3 was observed in any cell type. After cerulein treatment, increases in Smad3 and P-Smad3 were observed. Smad3 was observed mostly in the PSCs, whereas P-Smad3 was observed in the acinar cells and the PSCs. Halofuginone had no effect on the level of Smad3 protein expression, whereas complete elimination of P-Smad3 was observed after halofuginone treatment (Fig. 4).

Intracellular PSC Signaling Is Affected by Halofuginone

We evaluated the effect of halofuginone on the phosphorylation of key proteins in the MAPK pathways—JNK, MAPK/ERK, and p38 MAPK—and on Akt in PSCs derived from the control and the cerulein-treated pancreas (Fig. 5). Levels of phosphorylated JNK and, to a much lesser extent, phosphorylated MAPK/ERK were higher in the PSCs derived from the cerulein-treated pancreas relative to controls and were further increased after halofuginone treatment. Equal levels of phosphorylated Akt and p38 MAPK were observed in PSCs derived from control and cerulein-treated mice and were unaltered after halofuginone treatment.

Halofuginone Affects Cerulein-Dependent Acinar Cell Proliferation and PAP-1 Synthesis

Fully differentiated pancreatic acinar cells are capable of replication and can reenter the cell cycle to restore lost acinar tissue.[44] Only a small number of PCNA-positive acinar cells were detected in the untreated pancreas, whereas after cerulein treatment, a major increase in PCNA-positive cells was observed (Fig. 6). Halofuginone prevented this increase only in the early stages of pancreas fibrosis development. In pathologic situations, the acinar cells are the main source of PAP-1.[33] Almost no PAP-1 was synthesized by the control untreated pancreas or by the pancreas of mice treated with halofuginone alone. Cerulein caused increased PAP-1 synthesis, which was more evident after 4 weeks of treatment, and halofuginone caused a further increase in this synthesis (Fig. 7).

DISCUSSION

Chronic pancreatitis is characterized by pancreatic inflammation and fibrosis, eventually leading to destruction of pancreatic parenchyma and loss of exocrine and endocrine functions. In response to pancreatic injury or inflammation, PSCs are activated into highly proliferative myofibroblastlike cells that express smooth muscle proteins and produce ECM components. Administration of cerulein caused a major increase in the synthesis of fibrosis-related and TGFβ-dependent proteins such as collagen type I and P4Hβ (Fig. 1), consistent with other models of pancreatitis.[34,35] Halofuginone inhibited PSC activation, in agreement with previous observations of inhibition of HSC and tumor myofibroblast activation,[20,22,23] as evidenced by the following findings. (1) There was inhibition of synthesis of collagen type I, the major ECM protein, and of P4Hβ, the main enzyme responsible for its cross-linking (Fig. 1). The Sirius red staining that remained after halofuginone treatment may partly represent collagen type III, which also increases in pancreas fibrosis[35] but is not affected by halofuginone.[36] Halofuginone also inhibited collagen synthesis in severe hyperstimulation and obstruction pancreatitis in rats.[37] (2) There was inhibition of the expression of specific markers expressed in activated PSCs, such as Cygb/STAP, and of TGFβ-dependent increases in muscle-specific genes such as SM22α (Figs. 2A, B). (3) There was inhibition of PSC proliferation (Fig. 2C). All of the inhibited parameters are characteristic of activated PSCs. Transforming growth factor β is known to regulate PSC activation and to inhibit its proliferation. Although halofuginone inhibited TGFβ signaling, incubation of the PSC with halofuginone resulted in a dose-dependent inhibition of cell proliferation (Fig. 2C). These results suggest that halofuginone may have additional targets involved in cell proliferation, for example, within the MAPK signaling pathway (Fig. 5).

The course of chronic pancreatitis is characterized by recurrent episodes of acute pancreatitis, which cause parenchymal injury and necrosis, accompanied by fibrosis, chronic inflammation, and parenchymal cell loss, all of which increase with each successive episode. Hypoxia and hypoxia-related genes are upregulated during cerulein-induced acute pancreatitis.[38] It is interesting to note that the synthesis of Cygb/STAP and collagen P4Hβ is controlled by hypoxia.[39,40] Cytoglobin/stellate cell activation–associated protein is probably involved in cellular oxygen homeostasis and supply and plays a role as an oxygen reservoir that is used under hypoxic conditions to protect the tissue from oxidative stress.[41]

Regardless of the cause of the insult resulting in pancreas fibrosis, extensive ECM remodeling is required. In the first

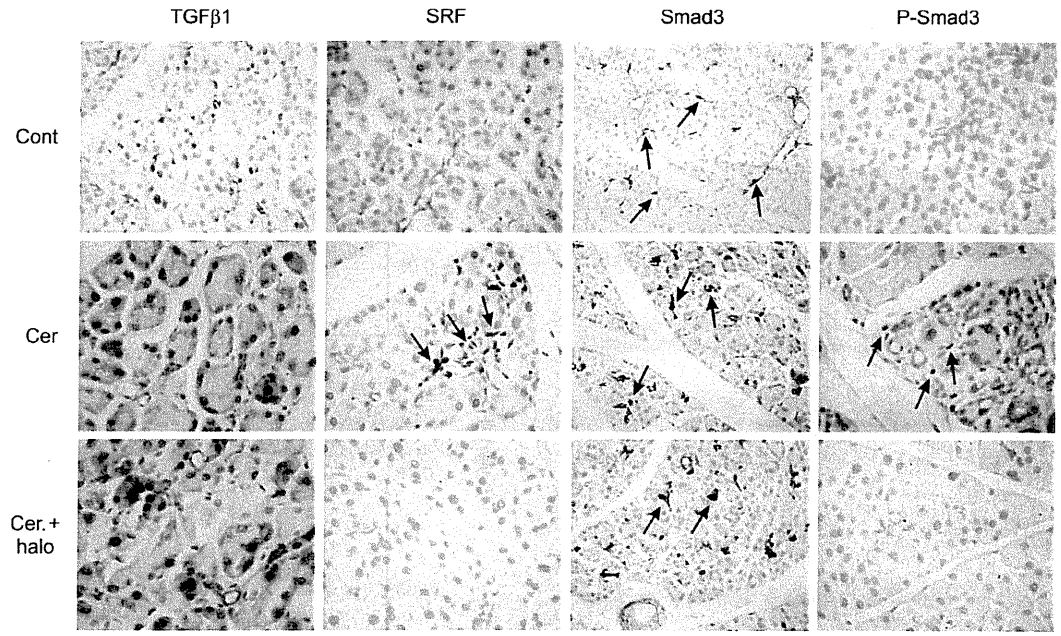

FIGURE 4. Halofuginone and TGFβ signaling. Transforming growth factor β, SRF, Smad3, and P-Smad3 levels were determined by immunohistochemistry in pancreas biopsies after 8 weeks of cerulein treatment, with or without halofuginone. Cells expressing the specific proteins are indicated by arrows. Note that halofuginone did not affect TGFβ levels but prevented the cerulein-dependent increases in SRF and P-Smad3, but not Smad3, levels.

step, transient local degradation of the ECM occurs, either by proteases of the plasminogen or by the MMP systems. The balance between the MMPs and their inhibitors is pivotal in the remodeling of the ECM. Tissue inhibitors of MMP-1 and TIMP2, derived from the activated PSCs,[16] are increased in the pancreas of cerulein-treated mice (Fig. 3A). Although both TIMPs are under the control of TGFβ, the regulation of TIMP1 is probably not Smad3-dependent. The Smad-containing complexes do not interact with the promoter-proximal activator protein 1 site of TIMP1 that is required for TGFβ activation; therefore, TGFβ was able to stimulate TIMP1 synthesis in a Smad-knockout cell line.[42] This could explain the observation that halofuginone, an inhibitor of Smad3 phosphorylation downstream of TGFβ signaling[21,23] (Fig. 4), inhibited only the synthesis of TIMP2 but not that of TIMP1 (Fig. 3A), as has been observed in chemically induced liver fibrosis.[20] Pancreatic stellate cells have the capacity to synthesize a number of MMPs under the control of TGFβ.[16] The PSCs derived from cerulein-treated mice exhibited much higher MMP-2 activity than those derived from the control mice, and the difference persisted even after several passages in culture (Fig. 3C). This may imply a fundamental genomic change while they are in the fibrotic tissue, or it may reflect the disparity in their origin. Halofuginone prevented the TGFβ-dependent increase in MMP-2 activity in both cell populations (Fig. 3D), but it increased MMP-3 activity only in the cells derived from cerulein-treated mice. These results are consistent with the effects of halofuginone on MMP activity observed in HSCs in culture and in rat hepatic-induced fibrosis.[43]

Transforming growth factor β is synthesized by the PSCs and was upregulated in the cerulein-treated pancreas (Fig. 4). Halofuginone, which has been found to overcome TGFβ-induced collagen synthesis without affecting TGFβ receptor expression,[23] did not affect TGFβ levels in the cerulein-treated mice, suggesting that halofuginone's target is probably downstream of the TGFβ-receptor interaction, along the Smad3 pathway. Indeed, halofuginone decreased the levels of P-Smad2/3 in the cerulein-treated pancreas without affecting the total level of Smad3, in agreement with previous findings.[21,23] Smad3, in conjunction with SRF, is a major mediator of TGFβ signaling, which results in transcription of smooth muscle–specific genes.[11] Serum response factor induces smooth muscle cell (SMC) gene expression, and the dominant-negative mutant of SRF blocks TGFβ-induced SMC genes.[44] In activated HSCs, TGFβ upregulates SRF synthesis, resulting in SMC gene expression.[45] The entire conditional inactivation of the SRF gene in the pancreas leads to severe pancreatitis,[46] although in the present study, in the cerulein-treated pancreas, SRF was upregulated exclusively by the PSCs, probably because of cerulein-dependent increases in TGFβ synthesis and Smad3 phosphorylation (Fig. 4). Halofuginone inhibited SRF synthesis without affecting the level of TGFβ, which again suggests that halofuginone inhibits smooth muscle gene expression and ECM production by inhibiting Smad3 phosphorylation downstream of TGFβ signaling, resulting in inhibition of PSC activation.

The PSCs derived from the pancreas of cerulein-treated mice exhibited much higher levels of phosphorylated JNK and, to a lesser extent, of MAPK/ERK, but not of p38 kinase or Akt. Halofuginone further increased JNK phosphorylation in the cerulein-treated PSCs. The JNK has been implicated as a repressor of TGFβ gene expression, and it contributes to the regulation of autocrine TGFβ-mediated biologic responses,[47] suggesting that there is cross-talk between the 2 signaling pathways. It is interesting to note that halofuginone causes increased phosphorylation of c-Jun transcription factor, a major JNK substrate, in Tsk/+ mouse fibroblasts in culture and in vivo, in correlation with a decrease in collagen synthesis.[48]

Halofuginone affects not only the stellate cells but also the epithelial cells of the tissue. In the liver, halofuginone stimulates insulin growth factor binding protein 1 synthesis by the hepatocytes, and the secreted insulin growth factor binding

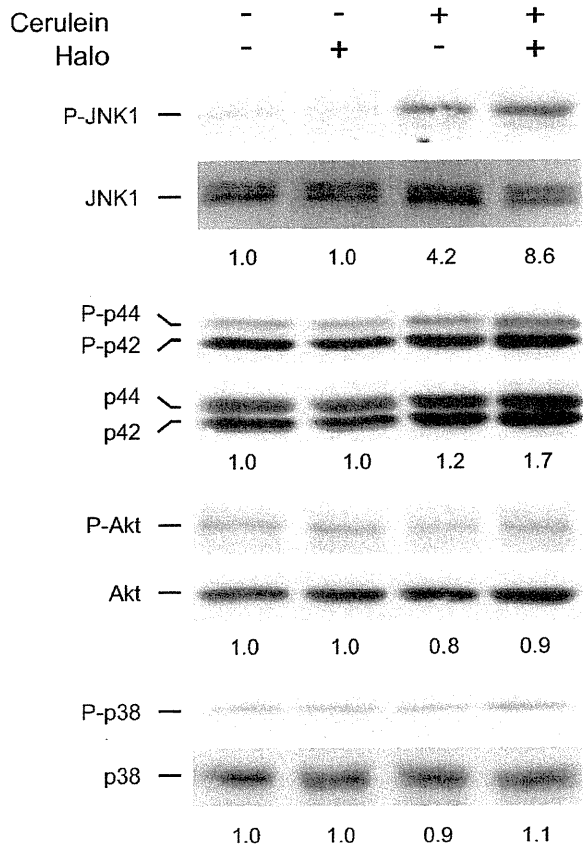

FIGURE 5. Halofuginone and JNK, MAPK, and Akt signaling in PSCs. Cells derived from the pancreas of control and cerulein-treated mice were cultured in the presence or absence of halofuginone (20 mmol/L). At the end of the incubation, cell extracts were blotted with the appropriate antibodies. Halofuginone further increased the cerulein-dependent phosphorylation of JNK and, to a lesser extent, the phosphorylation of MAPK/ERK. No effect of cerulein or halofuginone on Akt or p38 phosphorylation was observed.

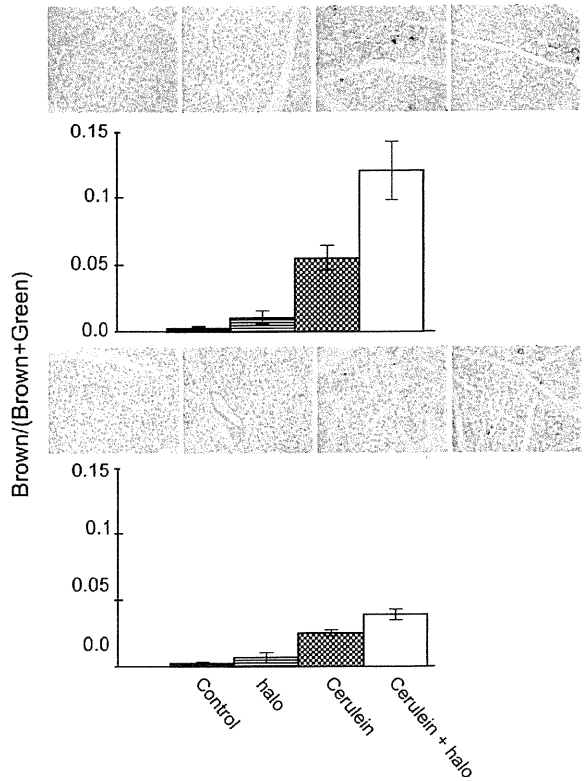

FIGURE 7. Halofuginone and PAP-1 synthesis. Pancreas biopsies were taken after 4 and 8 weeks of cerulein treatment, with and without halofuginone, immunostained with PAP-1 antibodies, and subjected to image analysis. In each panel, means without a common letter differ significantly ($P < 0.05$) according to Duncan multiple range test.

protein 1 inhibits HSC migration.[27] In the pancreas, PAP-1 is expressed at a level related to the severity of cerulein-induced pancreatitis in the acute phase.[49] Halofuginone prevented the cerulein-dependent increase in acinar cell proliferation and increased the synthesis of anti-inflammatory cytokine PAP-1 (Figs. 6, 7), which may further reduce PSC activation and matrix synthesis, by inhibiting inflammation. Halofuginone also inhibited rat inflammation after severe hyperstimulation and obstruction pancreatitis.[37]

In conclusion, we demonstrated that halofuginone prevents cerulein-dependent PSC activation by inhibiting Smad3

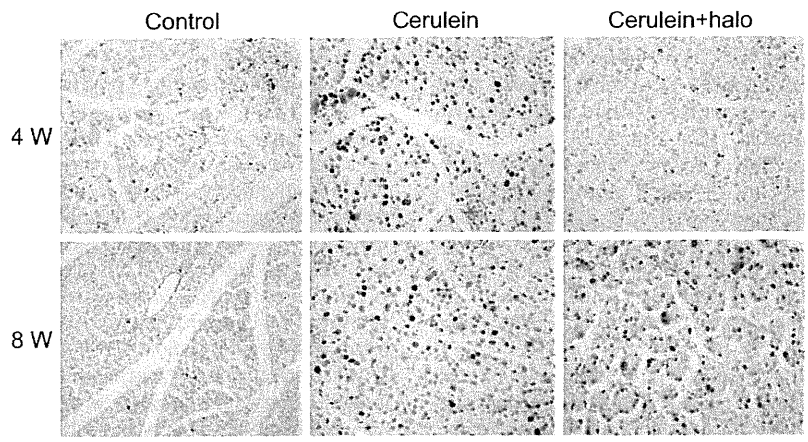

FIGURE 6. Halofuginone and acinar cell proliferation. Pancreas biopsies were taken after 4 and 8 weeks of cerulein treatment, with and without halofuginone, and were immunostained with PCNA antibodies. Halofuginone prevented the increase in acinar cell proliferation after only 4 weeks of treatment.

phosphorylation downstream of TGFβ signaling and via JNK phosphorylation. In addition, halofuginone increases the synthesis of the anti-inflammatory cytokine PAP-1 by the acinar cells, which can further reduce pancreas fibrosis. These results suggest that halofuginone, which has already exhibited human clinical efficacy[25,29] and is currently being evaluated in clinical trials for various indications,[50] could serve as a novel therapy for pancreas fibrosis.

ACKNOWLEDGMENT

This article is a contribution from the ARO, The Volcani Center.

REFERENCES

1. Witt H, Apte MV, Keim V, et al. Chronic pancreatitis: challenges and advances in pathogenesis, genetics, diagnosis, and therapy. *Gastroenterology.* 2007;132:1557–1573.
2. Kloppel G, Detlefsen S, Feyerabend B. Fibrosis of the pancreas: the initial tissue damage and the resulting pattern. *Virchows Arch.* 2004;445:1–8.
3. Apte MV, Wilson JS. Mechanisms of pancreatic fibrosis. *Dig Dis.* 2004;22:273–279.
4. Bachem MG, Schunemann M, Ramadani M, et al. Pancreatic carcinoma cells induce fibrosis by stimulating proliferation and matrix synthesis of stellate cells. *Gastroenterology.* 2005;128:907–921.
5. McCarroll JA, Phillips PA, Park S, et al. Pancreatic stellate cell activation by ethanol and acetaldehyde: is it mediated by the mitogen-activated protein kinase signaling pathway? *Pancreas.* 2003;27:150–160.
6. Nakatani K, Okuyama H, Shimahara Y, et al. Cytoglobin/STAP, its unique localization in splanchnic fibroblast-like cells and function in organ fibrogenesis. *Lab Invest.* 2004;84:91–101.
7. Apte MV, Phillips PA, Fahmy RG, et al. Does alcohol directly stimulate pancreatic fibrogenesis? Studies with rat pancreatic stellate cells. *Gastroenterology.* 2000;118:780–794.
8. Luttenberger T, Schmid-Kotsas A, Menke A, et al. Platelet-derived growth factors stimulate proliferation and extracellular matrix synthesis of pancreatic stellate cells: implications in pathogenesis of pancreas fibrosis. *Lab Invest.* 2000;80:47–55.
9. Yoo BM, Yeo M, Oh TY, et al. Amelioration of pancreatic fibrosis in mice with defective TGF-beta signaling. *Pancreas.* 1995;30:71–79.
10. Roberts AB, Russo A, Felici A, et al. Smad3: a key player in pathogenetic mechanisms dependent on TGF-beta. *Ann N Y Acad Sci.* 2003;995:1–10.
11. Qiu P, Feng XH, Li L. Interaction of Smad3 and SRF-associated complex mediates TGF-beta1 signals to regulate SM22 transcription during myofibroblast differentiation. *J Mol Cell Cardiol.* 2003;35:1407–1420.
12. Mack CP, Thompson MM, Lawrenz-Smith S, et al. Smooth muscle alpha-actin CArG elements coordinate formation of a smooth muscle cell–selective, serum response factor–containing activation complex. *Circ Res.* 2000;86:221–232.
13. Jesnowski R, Furst D, Ringel J, et al. Immortalization of pancreatic stellate cells as an in vitro model of pancreatic fibrosis: deactivation is induced by matrigel and *N*-acetylcysteine. *Lab Invest.* 2005;85:1276–1291.
14. Ishihara T, Hayasaka A, Yamaguchi T, et al. Immunohistochemical study of transforming growth factor-beta 1, matrix metalloproteinase-2,9, tissue inhibitors of metalloproteinase-1,2, and basement membrane components at pancreatic ducts in chronic pancreatitis. *Pancreas.* 1998;17:412–418.
15. Yokota T, Denham W, Murayama K, et al. Pancreatic stellate cell activation and MMP production in experimental pancreatic fibrosis. *J Surg Res.* 2002;104:106–111.
16. Phillips PA, McCarroll JA, Park S, et al. Rat pancreatic stellate cells secrete matrix metalloproteinases: implications for extracellular matrix turnover. *Gut.* 2003;52:275–282.
17. Omary MB, Lugea A, Lowe AW, et al. The pancreatic stellate cell: a star on the rise in pancreatic diseases. *J Clin Invest.* 2007;117:50–59.
18. Hwang RF, Moore T, Arumugam T, et al. Cancer-associated stromal fibroblasts promote pancreatic tumor progression. *Cancer Res.* 2008;68:918–926.
19. Erkan M, Kleeff J, Gorbachevski A, et al. Periostin creates a tumor-supportive microenvironment in the pancreas by sustaining fibrogenic stellate cell activity. *Gastroenterology.* 2007;132:1447–1464.
20. Bruck R, Genina O, Aeed H, et al. Halofuginone to prevent and treat thioacetamide-induced liver fibrosis in rats. *Hepatology.* 2001;3:379–386.
21. Gnainsky Y, Kushnirsky Z, Bilu G, et al. Gene expression during chemically induced liver fibrosis: effect of halofuginone on TGF-beta signaling. *Cell Tissue Res.* 2007;328:153–166.
22. Sheffer Y, Leon O, Pinthus JH, et al. Inhibition of fibroblast to myofibroblast transition by halofuginone contributes to the chemotherapy-mediated antitumoral effect. *Mol Cancer Ther.* 2007;6:570–577.
23. Pines M. Targeting TGFβ signaling to inhibit fibroblast activation as a therapy for fibrosis and cancer: effect of halofuginone. *Exp Opion Drug Discov.* 2008;3:1–10.
24. Pines M, Vlodavsky I, Nagler A. Halofuginone: from veterinary use to human therapy. *Drug Develop Res.* 2000;50:371–378.
25. Pines M, Snyder D, Yarkoni S, et al. Halofuginone to treat fibrosis in chronic graft versus host disease and scleroderma. *Biol Bl Marrow Transplant.* 2003;9:417–425.
26. Spira G, Mawasi N, Paizi M, et al. Halofuginone, a collagen type I inhibitor improves liver regeneration in cirrhotic rats. *J Hepatol.* 2002;37:331–339.
27. Gnainsky Y, Spira G, Paizi M, et al. Halofuginone—an inhibitor of collagen synthesis by rat stellate cells—stimulates insulin-like growth factor-binding protein 1 synthesis by hepatocytes. *J Hepatol.* 2003;40:269–277.
28. Gnainsky Y, Spira G, Paizi M, et al. The involvement of the tyrosine phosphatase early gene of liver regeneration (PRL-1) in cell cycle and in liver regeneration and fibrosis—effect of halofuginone. *Cell Tissue Res.* 2006;324:385–394.
29. Nagler A, Pines M. Topical treatment of cutaneous chronic graft versus host disease (cGvHD) with halofuginone: a novel inhibitor of collagen type I synthesis. *Transplantation.* 1999;68:1806–1809.
30. Keim V, Iovanna JL, Orelle B, et al. A novel exocrine protein associated with pancreas transplantation in humans. *Gastroenterology.* 1992;103:248–254.
31. Neuschwander-Tetri BA, Burton FR, Presti ME, et al. Repetitive self-limited acute pancreatitis induces pancreatic fibrogenesis in the mouse. *Dig Dis Sci.* 2000;45:665–674.
32. Kruse ML, Hildebrand PB, Timke C, et al. Isolation, long-term culture, and characterization of rat pancreatic fibroblastoid/stellate cells. *Pancreas.* 2001;23:49–54.
33. Closa D, Motoo Y, Iovanna JL. Pancreatitis-associated protein: from a lectin to an anti-inflammatory cytokine. *World J Gastroenterol.* 2007;13:170–174.
34. Koslowski R, Seidel D, Kuhlisch E, et al. Evidence for the involvement of TGF-beta and PDGF in the regulation of prolyl 4-hydroxylase and lysyloxidase in cultured rat lung fibroblasts. *Exp Toxicol Pathol.* 2003;55:257–264.

35. Miyauchi M, Suda K, Kuwayama C, et al. Role of fibrosis-related genes and pancreatic duct obstruction in rat pancreatitis models: implications for chronic pancreatitis. *Histol Histopathol*. 2007;22:1119–1127.
36. Choi ET, Callow AD, Sehgal NL, et al. Halofuginone, a specific collagen type I inhibitor, reduces anastomotic intimal hyperplasia. *Arch Surg*. 1995;130:257–261.
37. Karatas A, Paksoy M, Erzin Y, et al. The effect of halofuginone, a specific inhibitor of collagen type 1 synthesis, in the prevention of pancreatic fibrosis in an experimental model of severe hyperstimulation and obstruction pancreatitis. *J Surg Res*. 2008;148:7–12.
38. Gomez G, Englander EW, Wang G, et al. Increased expression of hypoxia-inducible factor-1alpha, p48, and the Notch signaling cascade during acute pancreatitis in mice. *Pancreas*. 2004;28:58–64.
39. Fähling M, Perlewitz A, Doller A, et al. Regulation of collagen prolyl 4-hydroxylase and matrix metalloproteinases in fibrosarcoma cells by hypoxia. *Comp Biochem Physiol C Toxicol Pharmacol*. 2004;139:119–126.
40. Fordel E, Thijs L, Martinet W, et al. Anoxia or oxygen and glucose deprivation in SH-SY5Y cells: a step closer to the unraveling of neuroglobin and cytoglobin functions. *Gene*. 2007;398:114–122.
41. Xu R, Harrison PM, Chen M, et al. Cytoglobin overexpression protects against damage-induced fibrosis. *Mol Ther*. 2006;13:1093–1100.
42. Hall MC, Young DA, Waters JG, et al. The comparative role of activator protein 1 and Smad factors in the regulation of Timp-1 and MMP-1 gene expression by transforming growth factor-beta 1. *J Biol Chem*. 2003;278:10304–10313.
43. Popov Y, Patsenker E, Bauer M, et al. Halofuginone induces matrix metalloproteinases in rat hepatic stellate cells via activation of p38 and NFkappaB. *J Biol Chem*. 2006;281:15090–15098.
44. Hirschi KK, Lai L, Belaguli NS, et al. Transforming growth factor-beta induction of smooth muscle cell phenotype requires transcriptional and post-transcriptional control of serum response factor. *J Biol Chem*. 2002;277:6287–6295.
45. Herrmann J, Haas U, Gressner AM, et al. TGF-beta up-regulates serum response factor in activated hepatic stellate cells. *Biochim Biophys Acta*. 2007;1772:1250–1257.
46. Miralles F, Hebrard S, Lamotte L, et al. Conditional inactivation of the murine serum response factor in the pancreas leads to severe pancreatitis. *Lab Invest*. 2006;86:1020–1036.
47. Ventura JJ, Kennedy NJ, Flavell RA, et al. JNK regulates autocrine expression of TGF-beta1. *Mol Cell*. 2004;15:269–278.
48. McGaha TL, Kodera T, Spiera H, et al. Halofuginone inhibition of COL1A2 promoter activity via a c-Jun–dependent mechanism. *Arthritis Rheum*. 2002;46:2748–2761.
49. Magaña-Gómez J, López-Cervantes G, Calderón de la Barca AM. Caerulin-induced pancreatitis in rats: histological and genetic expression changes from acute phase to recuperation. *World J Gastroenterol*. 2006;12:3999–4003.
50. de Jonge MJ, Dumez H, Verweij J, et al. EORTC New Drug Development Group (NDDG). Phase I and pharmacokinetic study of halofuginone, an oral quinazolinone derivative in patients with advanced solid tumours. *Eur J Cancer*. 2006;42:1768–1774.

Supplemental Material can be found at:
http://dmd.aspetjournals.org/content/suppl/2011/11/02/dmd.111.040923.DC1.html

1521-009X/12/4002-322–328$25.00
DRUG METABOLISM AND DISPOSITION
Copyright © 2012 by The American Society for Pharmacology and Experimental Therapeutics
DMD 40:322–328, 2012

Vol. 40, No. 2
40923/3743170

Prediction of In Vivo Hepatic Clearance and Half-Life of Drug Candidates in Human Using Chimeric Mice with Humanized Liver[S]

Seigo Sanoh, Aya Horiguchi, Kazumi Sugihara, Yaichiro Kotake, Yoshitaka Tayama, Hiroki Ohshita, Chise Tateno, Toru Horie, Shigeyuki Kitamura, and Shigeru Ohta

Graduate School of Biomedical Sciences (S.S., A.H., Y.K., S.O.) and Liver Research Project Center, Hiroshima University, Hiroshima, Japan (C.T.); Faculty of Pharmaceutical Sciences, Hiroshima International University, Hiroshima, Japan (K.S., Y.T.); PXB Mouse Production Department (H.O.) and R&D Department (C.T.), PhoenixBio Co., Ltd., Hiroshima, Japan; DeThree Research Laboratories, Ibaraki, Japan (T.H.); and Nihon Pharmaceutical University, Saitama, Japan (S.K.)

Received August 5, 2011; accepted November 2, 2011

ABSTRACT:

Accurate prediction of pharmacokinetics (PK) parameters in humans from animal data is difficult for various reasons, including species differences. However, chimeric mice with humanized liver (PXB mice; urokinase-type plasminogen activator/severe combined immunodeficiency mice repopulated with approximately 80% human hepatocytes) have been developed. The expression levels and metabolic activities of cytochrome P450 (P450) and non-P450 enzymes in the livers of PXB mice are similar to those in humans. In this study, we examined the predictability for human PK parameters from data obtained in PXB mice. Elimination of selected drugs involves multiple metabolic pathways mediated not only by P450 but also by non-P450 enzymes, such as UDP-glucuronosyltransferase, sulfotransferase, and aldehyde oxidase in liver. Direct comparison between in vitro intrinsic clearance ($CL_{int,in\ vitro}$) in PXB mice hepatocytes and in vivo intrinsic clearance ($CL_{int,in\ vivo}$) in humans, calculated based on a well stirred model, showed a moderate correlation ($r^2 = 0.475$, $p = 0.009$). However, when $CL_{int,in\ vivo}$ values in humans and PXB mice were compared similarly, there was a good correlation ($r^2 = 0.754$, $p = 1.174 \times 10^{-4}$). Elimination half-life ($t_{1/2}$) after intravenous administration also showed a good correlation ($r^2 = 0.886$, $p = 1.506 \times 10^{-4}$) between humans and PXB mice. The rank order of CL and $t_{1/2}$ in human could be predicted at least, although it may not be possible to predict absolute values due to rather large prediction errors. Our results indicate that in vitro and in vivo experiments with PXB mice should be useful at least for semiquantitative prediction of the PK characteristics of candidate drugs in humans.

Introduction

It is important to predict human pharmacokinetics (PK) and metabolism of drug candidates in the preclinical stage of pharmaceutical development. Various approaches to predict human clearance (CL) with in vitro metabolic systems, such as human liver microsomes and hepatocytes, have been reported (Nagilla et al., 2006; Brown et al., 2007; Fagerholm, 2007; Stringer et al., 2008; Chiba et al., 2009; Hallifax et al., 2010) but with limited success. One of the reasons for the discrepancy between predicted and observed CL may be that the preparation, storage, and experimental treatment of hepatocytes alter the normal function of metabolic enzymes (Wang et al., 2005). Although this might be ameliorated by using fresh hepatocytes immediately after isolation from the liver, these are not readily available and in any case show considerable interindividual differences.

It has become possible recently to predict CL and half-life ($t_{1/2}$) by means of computational approaches and physiologically based modeling (Ekins and Obach, 2000; De Buck et al., 2007; Tabata et al., 2009; Paixão et al., 2010). Accurate prediction of human PK is a key issue for the development of new drugs, because many new drug candidates with diverse chemical structures are metabolized not only by cytochrome P450 (P450) but also by non-P450 enzymes, such as UDP-glucuronosyltransferase (UGT) and sulfotransferase (SULT). It is also necessary to take into account the effects of cell permeability, transporter-mediated uptake, and excretion (Chiba et al., 2009; Huang et al., 2010).

Chimeric mice with humanized liver (PXB mice; PhoenixBio Co., Ltd., Hiroshima, Japan) have been generated from urokinase-type plasminogen activator/severe combined immunodeficiency mice transplanted with human hepatocytes (Tateno et al., 2004). In these mice, approximately 80% of the hepatocytes are human. The expression levels and metabolic activities of P450 and non-P450 enzymes in

This work was supported by a Grant-in-Aid for Young Scientists (B) from Japan Society for the Promotion of Science [Grant 22790109]; and PhoenixBio, Co., Ltd.

Article, publication date, and citation information can be found at http://dmd.aspetjournals.org.

http://dx.doi.org/10.1124/dmd.111.040923.

[S] The online version of this article (available at http://dmd.aspetjournals.org) contains supplemental material.

ABBREVIATIONS: PK, pharmacokinetics; CL, clearance; AO, aldehyde oxidase; $CL_{int,in\ vitro}$, in vitro intrinsic clearance; $CL_{int,in\ vivo}$, in vitro intrinsic clearance; CL_{oral}, oral clearance; CL_t, total clearance; P450, cytochrome P450; DMSO, dimethyl sulfoxide; fu, plasma unbound fraction; h-hepatocytes, PXB mice hepatocytes; LC/MS/MS, liquid chromatography tandem mass spectrometry; NAT, *N*-acetyltransferase; PXB mice, chimeric mice with humanized liver; *Q*, hepatic blood flow; Rb, blood/plasma concentration ratio; RI, replacement index; SULT, sulfotransferase; $t_{1/2}$, half-life; UGT, UDP-glucuronosyltransferase; AUC_{iv}, area under the concentration versus time curve by intravenous administration.

livers of PXB mice with a high replacement index (RI) are similar to those of humans (Katoh et al., 2004, 2005), and human-specific metabolites are formed in PXB mice (Inoue et al., 2009; Kaminura et al., 2010; Yamazaki et al., 2010; De Serres et al., 2011). Thus, PXB mice could be a good in vivo model for predicting drug metabolism in humans.

However, quantitative methods for predicting PK parameters of humans from data in PXB mice have not been established yet. Therefore, we selected 13 model compounds that are metabolized by P450 and/or non-P450 enzymes in liver and compared the PK parameters in humans and PXB mice, using both in vitro and in vivo approaches, to evaluate the utility of this animal model for the prediction of human PK.

Materials and Methods

Chemicals. 6-Deoxypenciclovir and mirtazapine were obtained from Toronto Research Chemicals Inc. (North York, ON, Canada). Dapsone, lamotrigine, salbutamol, and sulindac were purchased from Sigma-Aldrich (St. Louis, MO). Diclofenac was purchased from Tokyo Chemical Industry Co. Ltd. (Tokyo, Japan). Fasudil was obtained from Tocris Bioscience (Bristol, UK). (*S*)-Naproxen was purchased from Cayman Chemical (Ann Arbor, MI). Ibuprofen, ketoprofen, and (*S*)-warfarin were purchased from Wako Pure Chemicals (Osaka, Japan). Zaleplon was kindly provided by King Pharm. Inc. (Bristol, UK). All of the other regents and solvents were commercial products of the highest available grade or analytical grade.

Animals. The present study was approved by the animal ethics committee and was conducted in accordance with the regulations on the use of living modified organisms of Hiroshima University. PXB mice (10–14 weeks of age) with human hepatocytes were prepared by the reported method (Tateno et al., 2004). Human hepatocytes of a donor (African-American boy, 5 years old) were obtained from BD Biosciences (San Jose, CA). PXB mice were housed in a temperature- and humidity-controlled environment under a 12-h light/dark cycle.

The RI was determined by the measurement of human albumin in blood collected from the tail vein. The RI was estimated by the correlation curve between the human albumin levels in mouse blood and determined by using human-specific cytokeratin 8/18-immunostained liver sections (Tateno et al., 2004). The RI values of PXB mice used in this study ranged from 73.4 to 93.4%.

Administration. Drug solution (5 ml/kg) was administered intravenously to PXB mice at 0.3 to 5 mg/kg body weight. Solutions of dapsone, diclofenac, 6-deoxypenciclovir, fasudil, ketoprofen, ibuprofen, mirtazapine, naproxen, salbutamol, and sulindac were prepared in saline. In the cases of ketoprofen, ibuprofen, naproxen, and sulindac, equivalent amounts of alkali were added. Dapsone solutions contained 10% dimethyl sulfoxide (DMSO), and mirtazapine solutions were prepared with 10% DMSO and equivalent amounts of hydrochloric acid. Lamotrigine, and zaleplon solutions were prepared with 10% DMSO and 10% polyethylene glycol 400 in saline. Equivalent amounts of hydrochloric acid also were added to the solutions of lamotrigine and zaleplon. Warfarin was formulated in 3% DMSO and 97% saline with an equivalent amount of sodium hydroxide.

Blood samples after dosing were collected from orbital veins of PXB mice at predetermined times using heparinized glass. These samples were centrifuged, and the plasma was stored at −30°C.

Determination of Drug Concentrations in Plasma. A 10 μl aliquot of plasma was added to 40 μl of acetonitrile or methanol containing an internal standard (carbamazepine, ketoprofen, or ibuprofen). The mixtures were centrifuged at 14,000*g* for 5 min, and the supernatant was subjected to liquid chromatography tandem mass spectrometry (LC/MS/MS).

Isolation and Purification of Hepatocytes from PXB Mice. Fresh hepatocytes were isolated from PXB mice (13–15 weeks of age) by means of the in situ collagenase perfusion method and purified as described previously (Yamasaki et al., 2010). PXB mouse hepatocytes (h-hepatocytes) contained approximately 7% mouse hepatocytes. We used h-hepatocytes purified by the use of 66Z rat IgG and magnetic beads bearing anti-rat IgG antibodies. The magnetic removal of mouse hepatocytes reduced the level of mouse hepatocytes to approximately 2% (in this study, the purity of human hepatocytes from PXB mouse hepatocytes ranged from 96.6 to 99.7% after purification). Cell viability of the hepatocytes used in the experiments ranged from 79 to 91%, as determined by means of the trypan blue exclusion test.

In Vitro Metabolic Studies Using h-Hepatocytes. The h-hepatocyte suspension (1×10^6 cells/ml) was incubated in Krebs-Henseleit buffer without serum in the presence of 10 μM of the test drug at 37°C under an atmosphere of 5% CO_2/95% O_2. The final concentration of acetonitrile was 0.5% (v/v) in the reaction mixture. The plates (24 wells) were shaken gently with an orbital shaker. The incubation mixture was sampled at 0, 0.25, 0.5, 1, and 2 h after treatment, and reactions were stopped by freezing the mixture in liquid nitrogen. When required, the samples were thawed, spiked with two volumes of acetonitrile or methanol containing an internal standard, and centrifuged. Aliquots of the supernatants were subjected to LC/MS/MS.

LC/MS/MS Conditions. Aliquots (10 μl) of plasma and h-hepatocyte suspension were introduced into the high-performance liquid chromatography system with an autosampler (Agilent Technologies, Santa Clara, CA). Several mobile phase conditions were used. Mobile phase condition 1 consisted of 10 mM ammonium acetate (A) and acetonitrile (B) on an Inertsil ODS-3 column (3 μm, 50 × 2.1 mm; GL Sciences Inc., Tokyo, Japan) at 40°C for the analysis of diclofenac, ibuprofen, ketoprofen, mirtazapine, (*S*)-naproxen, sulindac, and (*S*)-warfarin. The flow rate was set at 0.2 ml/min. The starting condition for the high-performance liquid chromatography gradient was 90:10 (A/B). From 0 to 5 min, the mobile phase composition was changed linearly to 10:90 (A/B), and this was held until 8 min. The gradient then was returned to 90:10 (A/B)

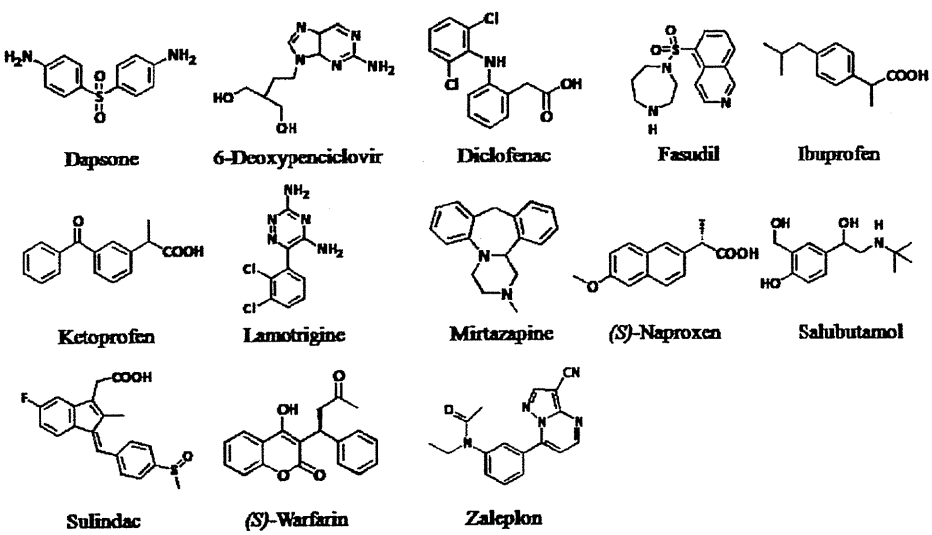

FIG. 1. Chemical structures of the model compounds used in this study.